This is to certify that the
thesis entitled

Thermal conductivity measurements of bulk materials and thin films by the 3ω method

presented by

Romy Liske

has been accepted towards fulfillment
of the requirements for the

M.S. degree in Material Science Engineering

Eldon D. Case
Major Professor's Signature

August 15, 2005
Date

THERMAL CONDUCTIVITY MEASUREMENTS OF BULK MATERIALS AND THIN FILMS BY THE 3ω METHOD

By

Romy Liske

A THESIS

Submitted to
Michigan State University
In partial fulfillment of the requirements
for the degree of

MASTER OF SCIENCE

Department of Material Science and Chemical Engineering

2005

ABSTRACT

THERMAL CONDUCTIVITY MEASUREMENTS OF BULK MATERIALS AND THIN FILMS BY THE 3ω METHOD

By

Romy Liske

An experimental apparatus was assembled based on a four-wire 3ω method to determine the thermal conductivity of bulk and thin film materials. By driving a current of angular frequency ω through a thin heating wire deposited on a specimen surface, a localized thermal wave with a frequency 2ω is created. Due to the change of the metal line's resistance with increasing temperature the imposed temperature oscillation can be estimated by measuring the voltage drop at a frequency 3ω. The 3ω measurements were performed in a frequency range covering five orders of magnitude (1 Hz – 300 kHz).

Bulk materials with a low thermal conductivity (soda lime with 1.15 W/(m·K) and Pyrex with 1.33 W/(m·K)) as well as silicon that possesses a much higher thermal conductivity (130 W/(m·K)) were measured by the 3ω method. In addition, the thermal conductivities of silica films of thicknesses between 0.3 μm to 3.2 μm were measured. The determined thermal conductivity of those silica films (1.55 W/(m·K)) was independent of film thickness. Finally, the possibility of measuring the thermal conductivity of thin diamond films is discussed.

ACKNOWLEDGEMENTS

Especially, I would like to thank Professor Eldon D. Case for thesis direction, his patience, thoughtful commentary and support. Without Professor Case this thesis would not exist.

My appreciation goes to my other committee members as well: Professor Subramanian and Professor Mueller. Thank you very much not just for being on my committee but for all of your guidance and assistance.

I owe a great deal to staff and students of the MSU Material Science Department, without whose cooperation and willingness to be inconvenienced this work would not have been possible.

My gratitude to my co-workers in the Fraunhofer Center and in the Engineering Research Center for helping to make this thesis a reality. In particular, I would like to thank:

- Professor Timothy Hogan (Electrical and Computer Engineering Department, Michigan State University) and his group for providing the initial 3ω background information, and for providing the probe station as well as the lock-in amplifiers,
- Professor Timothy Grotjohn (Electrical and Computer Engineering Department, Michigan State University) for his advice in all electrical issues and his guidance in assembling the experimental apparatus,
- Thomas Wunderer for assembling the compensation circuit,

- Syed Ahmed for always offering a helping hand and his support in the day-to-day project work, and
- Fraunhofer CCL for establishing and funding the project.

A very special word of thanks goes to a great friend and colleague, Michael Leonhardt, for going this journey with me, for supporting dR/dT-measurements even on weekends, for carrying out laser acoustic measurements, and for all his assistance.

I am grateful for the patience of my friends in overseas. Thank you for repeatedly calling, when I missed my turns, for talking and for listening, and for making my vacations back home unforgettable.

Most of all, I would like to thank my family, and especially my parents, for their absolute confidence in me. The knowledge that they would always be there to pick up the pieces is what allowed me to risk getting shattered.

TABLE OF CONTENTS

LIST OF TABLES

LIST OF FIGURES

1 Introduction

In the past years, the field of applications for thin films constantly increased. Thin films function as protection layers, hard or decorative coatings or optical coatings [1]. Either in form of single or multi layers, the term "thin" films covers thicknesses from a few Angstroms to tens of microns. In microelectronics electrical circuits or sensors are entirely built by stacking and structuring thin films, as well as diode and miniature solid-state are made of thin films [1]. Among other things, the reliability of electronic devices or coated materials depends on heat transport and conduction especially when high power or high temperature levels are involved [2].

The thermal conductivity has been investigated sufficiently for most materials on the market. Although these literature values of thermal conductivity are a good indication of how well a material conducts heat in general, those values should be considered as "bulk values" assuming an ideal and infinite thick material. Properties of thin films can differ from that of bulk materials with respect to their microstructure and chemical constitution [3]. Furthermore, thin films are characterized by their large surface to volume ratio. In addition boundary and interface scattering become important issues for conducting heat [4, 5, 6]. Thermal conductivity measurements of thin films directly can provide helpful information about the relationship between thermal properties and film

composition, thickness or structure. The measurements also provide a helpful tool to enhance the search for suitable materials for thin film applications.

In 1987 Cahill and co-workers introduced a method (named 3ω method) that allows thermal conductivity measurements of dielectric materials [7]. The Cahill technique involves depositing a thin rectangular metal line on a sample using lithography and metal evaporation. Applying an alternating current of frequency ω to the metallic line creates a periodic semi-cylindrical heat wave which diffuses into the substrate. The heat wave is exponentially damped in the radial direction, whereby the degree of damping is associated with the ability of the underlying material to conduct thermal energy. A material of low thermal conductivity exhibits a short damping distance, while a material with high thermal conductivity transmits the heat wave over a longer distance. The metal line experiences a temperature oscillation at 2ω, twice of the exciting frequency. Since the resistance of a metal is temperature dependent, the amplitude of the temperature oscillation can be determined by measuring the change in resistance of the metal line. It can be shown, that the temperature oscillation amplitude is proportional to a voltage drop at 3ω, which is three times the input frequency [7]. By measuring the 3ω voltage as a function of excitation frequency by a lock-in amplifier technology, the thermal conductivity of the substrate can be determined.

Unlike the hot-wire technique [8, 9, 10], where a step function of power is applied to a wire and the change of resistance is recorded as a function of time, the 3ω

method has the advantage of moving the measurement into the frequency domain. Hence, the long equilibration times required for the hot-wire technique are reduced to a few periods of temperature oscillation for the Cahill technique.

Initially, the 3ω method was used to measure the thermal conductivities of materials exhibiting low values. In those materials the damping distance of the heat wave is small resulting in a high temperature amplitude of the metal line. Therefore, the resistance of the metal will change significantly, resulting in a strong dependency of the 3ω voltage on the excitation frequency. An improved lock-in amplifier technology enables the detection of small changes in the 3ω voltage with high accuracy. This has the advantage of extending the measurements to materials of high thermal conductivities.

The 3ω method probes the sample to a depth q^{-1} referred to as the penetration depth or more precisely the damping distance of the thermal wave. The parameter q^{-1} is a function of the thermal conductivity and the frequency ω. Low frequencies allow the thermal wave to penetrate deeply into the substrate, while high frequencies lead to a reduced penetration depth allowing the measurement of thin films.

2 Theory of thermal conductivity

In a solid heat is transported by atomic lattice vibrations (called phonons) and by charge carries (electrons and holes). The contribution of charge carries to the thermal conductivity is the reason, why materials that are good electrical conductors, such as metals, are also good thermal conductors.
Compared to metals, electrical insulators do not exhibit free electrons due to covalent (or ionic) bonding. Thus, heat conduction in dielectric materials is due to lattice vibrations.
The bonds between atoms in a solid crystal are not rigid, but act like springs creating a spring-mass system. When an atom or plane of atoms is displaced, this displacement can travel as a wave through the crystal, transporting energy as it propagates.

Considering phonons as a gas of particles, the thermal conductivity can be derived from gas kinetics [11].
A gas between two plates of different temperatures T_1 and T_2 has a temperature gradient along the y-direction, dT/dy (Figure 1).

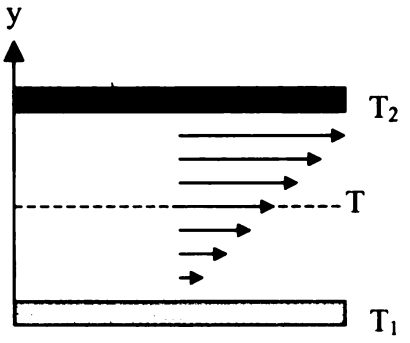

Figure 1. Gas between two plates of different temperatures (adapted from [11])

Let T be a temperature between the two plates (demonstrated by a dotted line in Figure 1) where the gas particles have a kinetic energy $\overline{w}$,

$$\overline{w} = \frac{f}{2} NkT \tag{1}$$

where

f - Degree of freedom

N - Number of gas particles

k - Boltzmann's constant.

The number of molecules per unit time crossing a unit area of the dotted line from either side is $\frac{1}{4} n\bar{v}$, where $\bar{v}$ denotes the mean velocity of the gas particles [12]. It can be shown that, on the average, each molecule crossing the dotted line makes its last collision at a height $\overline{y}$ equal to two-thirds of the mean free path of the gas particles, λ.

$$\bar{y} = \pm \frac{2}{3} \lambda \,. \tag{2}$$

At a height $\bar{y}$ above or below the dotted line in Figure 1 the temperature of the gas is given by

$$T^{\pm} = T \pm \frac{2}{3} \lambda \frac{dT}{dy} \,. \tag{3}$$

From equation 1, the energy carried across the dotted line by the gas particles becomes

$$\overline{w}^{\pm} = \frac{1}{4} n\bar{v} \cdot \frac{f}{2} k\left(T \pm \frac{2}{3}\lambda \frac{dT}{dy}\right). \tag{4}$$

The net rate of energy flow per unit area is the difference between the energy that is carried by particles crossing the plane from above and the energy that is carried by particles crossing the plane from below

$$H = \overline{w}^{+} - \overline{w}^{-} = \frac{1}{6} n\bar{v} f k \lambda \frac{dT}{dy}. \tag{5}$$

The energy flow *H* is similar to the heat flowing across an area per unit time. By definition, the heat flow and the temperature gradient *dT/dy* are related to each other by the thermal conductivity *K*.

$$H = K \frac{dT}{dy}. \tag{6}$$

Thus, *K* is given by

$$K = \frac{f}{6} n\bar{v} k \lambda. \tag{7}$$

Similar to the gas kinetics, where heat is transported by gas particles, in dielectric solids, heat is conducted by phonons. By introducing the heat capacity of phonons as $C = ½ f k n$ (Dulong Petit Law), v as the phonon velocity and λ as the

phonon mean free path, the thermal conductivity for a dielectric material becomes [13]

$$K = \frac{1}{3} C v \lambda \quad . \tag{8}$$

When discussing heat transport in solids by phonons, an important factor is the degree to which these lattice waves are disrupted, or scattered. Phonons can be scattered by defects or dislocations in the crystal, crystal boundaries, impurities such as dopants or alloying species, or by interactions with other phonons. These scattering mechanisms can be grouped into two categories: elastic scattering and inelastic scattering. An important metric in the discussion of phonon scattering mechanisms is the phonon mean free path λ, which is the average distance a phonon travels between collision.

In an ideal, infinite crystal, lattice vibrations are purely harmonic and do not interact with each other. Without collisions between phonons, the phonon mean free path would be infinite resulting in an infinite thermal conductivity. However, in non-ideal crystals with an-harmonic lattice interactions, the phonon mean free path is limited due to phonon-phonon interactions [13].
Phonon-phonon interactions are divided into elastic collisions and inelastic collisions, called "normal" and "umklapp" processes, respectively.
In a normal scattering process, two phonons with wave vectors $\vec{k_1}$ and $\vec{k_2}$ combine to form a third wave vector $\vec{k_3}$.

$$\vec{k_1} + \vec{k_2} = \vec{k_3} \quad (9)$$

In normal processes the phonon momentum is unchanged. Due to the conservation of the phonon momentum, elastic collisions do not produce any resistance to the heat flow [12].

The finite thermal conductivity of solids is due to the existence of umklapp processes in which the phonon momentum is not conserved

$$\vec{k_1} + \vec{k_2} = \vec{k_3} + \vec{G} \quad (10)$$

The reciprocal lattice vector $\vec{G}$ reverses the direction of the phonon which slows down the mass transport of heat [12]. Thus, the mean free path λ related to the thermal conductivity in equation 8 is the mean free path between umklapp collisions.

At low temperatures the umklapp process drastically decreases due to the reduced number of phonons. Hence, the phonon mean free path increases until it reaches the dimensions of crystal. However, the thermal conductivity may not increase, because of the temperature dependent heat capacity C in equation 8. The heat capacity C varies as T^3 at low temperatures. Therefore, the thermal conductivity K will decrease towards lower temperatures whenever the phonon mean free paths becomes comparable with the crystal size [13].

At high temperatures the number of phonons increases which results in a shorter mean free path lengths. This in turn increases the probability for the occurrence

of umklapp processes. The thermal conductivity at high temperatures will be inversely proportional to temperature [12].

Lattice imperfections may also reduce the phonon mean free path. Phonon scattering can occur due to crystal boundaries, atomic mass deviations due to isotopic elements, chemical impurities, and vacancies [13, 14, 15].

3 Mathematical background of the 3ω method

When an electrical current of $I(t) = I_0 \cos(\omega t)$ is supplied by two contact pads, the electrical power input, *P(t)*, is given by

$$P(t) = I_0^2 \cos^2(\omega t) \cdot R = \frac{1}{2} I_0^2 R[1 + \cos(2\omega t)] \quad (11)$$

Equation 11 can be split into two terms, one frequency independent term and one frequency dependent term [16].

$$P(t) = \left(\frac{1}{2} I_0^2 R\right)_{DC} + \left(\frac{1}{2} I_0^2 R \cos(2\omega t)\right)_{2\omega} \quad (12)$$

The dissipation of electrical energy generates a temperature increase in the metal strip. The temperature change also consists of a frequency dependent as well as frequency independent term.

$$T(t) = T_{DC} + T_{2\omega} \cos(2\omega t + \phi) \quad (13)$$

The T_{DC} term describes a temperature increase caused by steady state or joule heating while $T_{2\omega}$ is the temperature oscillation at a frequency twice of the input frequency.

An increase in temperature will cause a material specific change in resistance. By knowing the *dR/dT* behavior of the metal strip either from tabulated values or

from measurements, the strip can be used both as heater and also as thermometer.

The constant α is defined as the relative change of resistance versus temperature.

$$\frac{dR}{dT} = R_0 \alpha \quad . \tag{14}$$

Therefore the temperature dependent resistance of a metal can be written as

$$R = R_0 (1 + \alpha T(t)) \quad . \tag{15}$$

Combining equations 13 and 15 gives a relationship for the oscillation in resistance with a frequency of 2ω.

$$R = R_0 (1 + \alpha T_{DC} + \alpha T_{2\omega} \cos(2\omega t + \phi)) \quad . \tag{16}$$

Both, the applied current and the resistance of the metal are connected by the voltage drop across the strip.

$$V(t) = I(t) \cdot R \quad . \tag{17}$$

Expressing the current as $I(t) = I_0 \cos(\omega t)$ and using equation 16 the voltage then can be written as

$$V(t) = I_0 \cos(\omega t) \cdot R_0 (1 + \alpha T_{DC} + \alpha T_{2\omega} \cos(2\omega t + \phi)) \quad . \tag{18}$$

Rearranging equation 18 gives a 3ω term, after which the measuring method was named [16].

$$V(t) = (1 + \alpha T_{DC}) R_0 I_0 \cos(\omega t) + \frac{\alpha T_{2\omega} R_0 I_0}{2} \cos(\omega t + \phi) + \frac{\alpha T_{2\omega} R_0 I_0}{2} \cos(3\omega t + \phi) \quad . \quad (19)$$

The first two terms of equation 19 describe the voltage drop across the metal strip due to joule heating at an applied frequency 1ω. The last term in equation 19 adds a voltage at a frequency 3ω, from which the temperature oscillation $T_{2\omega}$ can be estimated [16].

$$T_{2\omega}(\omega) = \frac{2V_{3\omega}}{\alpha R_0 I_0} = 2 \cdot \frac{V_{3\omega}}{V_{1\omega}} \frac{dT}{dR} R_0 \quad . \quad (20)$$

By measuring the first harmonic and third harmonic voltage as well as the relative change of resistance of the metal versus temperature, the temperature oscillation can be determined as a function of frequency.

The temperature oscillation of the metal strip can be related to the thermal conductivity of the material underneath the heater/thermometer line using a solution adapted from work by Cahill and co-workers.

We begin with Carslaw and Jäger's solution for temperature change induced in an infinite solid heated by a thin wire carrying electric current [17].

$$\Delta T = \frac{P}{4\pi l K} \int_{-\infty}^{t} e^{\frac{i\omega t' - r^2}{4D(t-t')}} \frac{dt'}{t-t'} \quad . \quad (21)$$

Equation 21 holds for a periodic line source heated with by an electrical power per unit length P/l from time $t = -\infty$ to $t = t'$ with r being the radial distance from the line given by

$$r = \sqrt{x^2 + y^2}\,. \tag{22}$$

Laplace transformation of the integral term gives K_0, a zeroth order Bessel function of the second kind, which gives

$$\Delta T = \frac{P}{2\pi l \lambda} K_0(qr)\,. \tag{23}$$

The reciprocal of the wave vector q defines the wavelength of the thermal heat wave generated by electrical heating [18], such that

$$q^{-1} = \sqrt{\frac{D}{i\omega}}\,. \tag{24}$$

The wavelength q^{-1} is often referred as the penetration depth of the heat wave, although damping distance might be more accurate. The magnitude of q^{-1} is an important parameter for designing the 3ω method to probe materials of different thicknesses. As equation 24 shows the penetration depth of the thermal wave into a material decreases with increasing frequency. In addition the penetration depth is associated with the thermometric (or thermal) diffusivity D of a material. Thermal diffusivity D and thermal conductivity K are related to each other by the density ρ and heat capacity C of a material [18].

$$D = \frac{K}{\rho C}. \tag{25}$$

For the 3ω method, temperature oscillation is detected at the metal/sample interface by a metal line of the line width *2b*. Therefore, only the temperature gradient in the *x*-direction (along the sample surface) is important and for further estimates of thermal conductivity thermal oscillations on the *y*-direction are neglected. Ignoring the *y*-direction temperature oscillations implies the assumption of a specimen that is isotropic in the *x*-*y* plane. The penetration depth of the thermal wave in *x* and *y* direction is assumed to be equal, which is in fact only true for isotropic and homogenous materials. Furthermore, the thickness of the metal line itself is neglected.

Equation 23 is transformed to Cartesian coordinates, and then the real space coordinate *x* is replaced by the Fourier space *k* [19] to give

$$\Delta T(x) = \frac{P}{l\pi K} K_0(qx) = \frac{P}{l\pi K} \int_0^\infty \frac{\cos(qxt)}{\sqrt{t^2+1}} dt = \frac{P}{l\pi K} \int_0^\infty \frac{\cos(kx)}{\sqrt{k^2+q^2}} dk \tag{26a}$$

In general, $e^{ikx} = \cos(kx) + i\sin(kx)$. (26b)

The Fourier transform can be written as

$$\Delta T(x) = \frac{1}{\sqrt{2\pi}} \int_{-\infty}^{\infty} \Delta T(k) \cdot e^{ikx} dk$$

$$= \frac{1}{\sqrt{2\pi}} \int_{-\infty}^{\infty} \Delta T(k) \cdot \cos(kx) dk + \frac{i}{\sqrt{2\pi}} \int_{-\infty}^{\infty} \Delta T(k) \cdot \sin(kx) dk \quad . \tag{27}$$

Since equation 26 is a symmetric function, the Fourier transformation can be simplified to

$$\Delta T(x) = \sqrt{\frac{2}{\pi}} \int_{0}^{\infty} \Delta T(k) \cdot \cos(kx) dk \quad . \tag{28}$$

Replacing $\Delta T(x)$ in equation 16 with equation 28 and rearranging for $\Delta T(k)$ yields [20]

$$\Delta T(k) = \frac{P}{\sqrt{2\pi} l \lambda} \cdot \frac{1}{\sqrt{k^2 + q^2}} \quad . \tag{29}$$

Assuming heat enters the sample uniformly across the line width *2b* the Fourier transformation of the finite heat source of line width *2b* can be written as

$$\frac{1}{2b} rect\left(\frac{x}{2b}\right) \quad \mapsto \quad \frac{\sin(kb)}{kb} \quad . \tag{30}$$

The finite width of the metal line is included by taking the product of equation 28, after *ΔT(k)* was substituted by equation 29, and equation 30. Then, the inverse transformation is used to get

$$\Delta T(x) = \frac{P}{l\pi K}\int_0^{\infty} \frac{\sin(kb)\cos(kx)}{kb\sqrt{k^2+q^2}}\,dk \qquad (31)$$

Finally, equation 31 is integrated over the line width $-b < x < b$ and averaged by dividing by $2b$ [20].

$$\Delta T = \frac{P}{l\pi K}\int_0^{\infty} \frac{\sin^2(kb)}{(kb)^2\sqrt{k^2+q^2}}\,dk \qquad (32)$$

Equation 32 gives a general solution for the total temperature oscillation on a surface caused by a heat source of finite width $2b$ assuming one dimensional heat flow or an isotropic material, and neglecting the thermal boundary resistance between metal line and sample.

Figure 2 schematically shows the curvature of the temperature oscillation based on equation 32 and the relationship between frequency and penetration depth of the thermal wave.

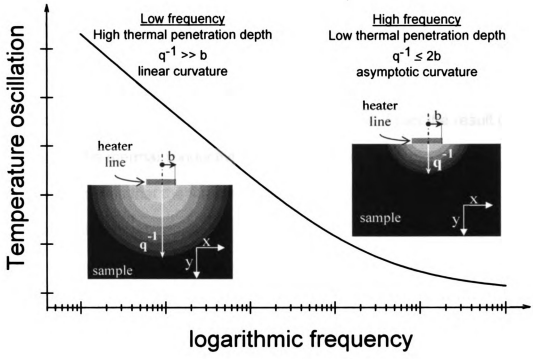

Figure 2. Schematics of the temperature oscillation as a function of frequency assuming infinite sample thickness *t*

3.1 Measurements on bulk materials

The principal curvature of the temperature oscillation for an infinite thick sample shown in Figure 2 can be divided into two regions. In the first region, the thermal penetration depth is much larger than the heater width *2b*. Therefore, the temperature oscillation is nearly linear versus logarithmic frequency. The linear curvature can be described by approximating equation 32. From the result of this approximation, the thermal conductivity can be determined by the "slope method", which states that the thermal conductivity is inversely proportional to the slope of the linear curvature.

In the second region, the penetration depth of the thermal wave is in the order of the line width *2b* or smaller than *2b*. In this case, the temperature oscillation shows an asymptotic curvature. Since an analytical solution for equation 32 in the asymptotic region is unknown [21], extracting the thermal conductivity from the temperature oscillation versus frequency plot is carried out by fitting equation 32 to measured data with the help of appropriate software.

3.2 Slope Method

Cahill [22] explored an approximation for the case, that the thermal wavelength is much larger than the line width, $q^{-1} >> b$. This approximation is appropriate for 3ω voltage measurements at low frequencies, where the thermal wave is allowed to penetrate deep into the underlying material (left part of Figure 2).

Using a series expansion of the Bessel function and truncating the series in the limit $|qr| << 1$ equation 23 can be approximated by [7]:

$$\Delta T = \frac{P}{l\pi K}\left(-\frac{1}{2}\ln(2\omega) - \ln\left(\frac{ib^2}{D}\right) + \ln 2 - \frac{i\pi}{4} - \gamma\right) = \frac{P}{l\pi\lambda}\left(-\frac{1}{2}\ln(2\omega) + const\right) \quad (33)$$

where $\gamma = 0.5772...$ is Euler's constant.

Substituting ΔT with the temperature oscillation derived in equation 10 and considering the slope $\frac{dV_{3\omega}}{df}$ in order to eliminate the constant term, the thermal conductivity can be calculated from [23]:

$$\lambda = \frac{V_{1\omega}^3}{4\pi l R_0^2\left(\frac{dV_{3\omega}}{df}\right)}\frac{dR}{dT} \quad . \quad (34)$$

For a linear slope $\frac{dV_{3\omega}}{df}$ measuring the third harmonic voltage at two different frequencies should be sufficient to calculate the thermal conductivity K [7]. In practice, data are taken over a wide range of frequencies and the slope of a temperature oscillation versus frequency regression line is used rather than the 3ω voltage at only two frequencies.

It should be pointed out that the linear approximation only holds when the penetration depth of the thermal wave is much larger than the width of the metal line. Otherwise the curvature of the temperature oscillation versus the logarithm of the heater frequency no longer follows a straight line (see Figure 2).

3.3 Measurements on two-layer systems

The curvature of the temperature oscillation versus frequency for a sample exhibiting a coating of lower thermal conductivity is schematically shown in Figure 3. In general, the plot can be divided into two parts. For high frequencies, the penetration depth of the thermal wave is low. As long as the thermal penetration depth q^{-1} is smaller than the coating thickness t the temperature oscillation contributes to the coating. The shape of the curvature depends on the ratio of heater line width $2b$ and film thickness t as described in section 3.1. The curvature is mainly asymptotic if the coating thickness is comparable with the line width. If the coating thickness is higher than the line width $2b$, the curvature will consist of a linear region.

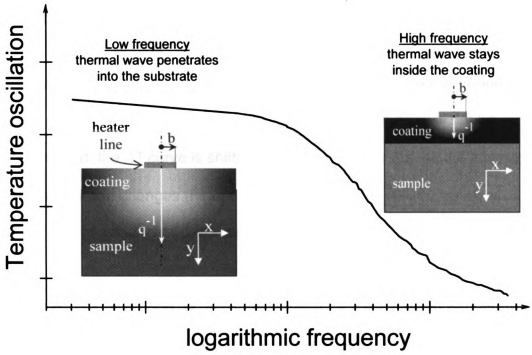

Figure 3. Schematic curvature of the temperature oscillation for a coated sample showing the low frequency region where the offset model applies (Figure 2) and the high frequency region that contributes to the coating.

3.4 Offset Method

Consider a sample that is coated with a low thermal conductivity film where the film thickness t is small compared to the metal line width $2b$. In this case, the heat flow inside the coating can be assumed to be one dimensional. Since the thermal wavelength is much larger than the film thickness for the low frequency range, the slope of the temperature oscillation versus frequency will not be affected. Instead, the ΔT curve is shifted up by a constant value as the intercept of our linear function changes (Figure 4) [22].

That offset can be used to calculate the thermal conductivity of the coating.

Combining equations 33 and 34 gives the solution for a normalized temperature oscillation

$$\frac{8l\pi V_{3\omega}R_0^2}{V_{1\omega}^3\, dR/dT} = -\frac{1}{K_{substrate}}\ln f + \frac{\ln\left(\frac{2D}{\pi b^2}\right)}{K_{film}} \quad (35)$$

Solving for ΔT explicitly gives

$$\Delta T_{total} = -\frac{1}{K_{substrate}}\ln f + \frac{\ln\left(\frac{2D}{\pi b^2}\right)}{K_{film}} \quad (36)$$

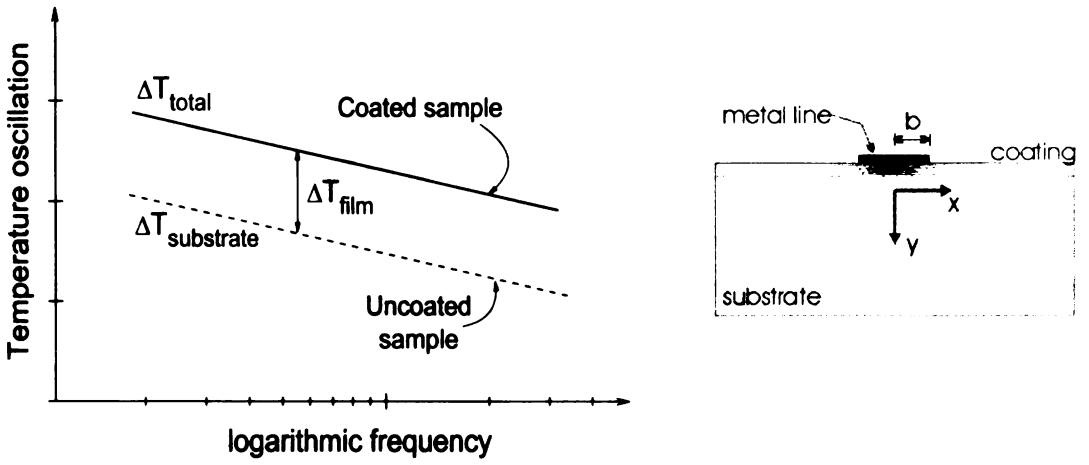

Figure 4. Left: Schematic curvature of the temperature oscillation for a coated sample. Right: Cross section of the heater and sample geometry for a coated substrate.

Equations 35 and 36 are valid for the low frequency region, where the temperature oscillation versus logarithmic frequency follows a straight line. The slope of the total temperature oscillation ΔT_{total} is related to the thermal conductivity of the substrate $K_{substrate}$ (as discussed in section 3.1). The slope is not influenced by the thermal conductivity of the coating K_{film} in contrary to the intercept of the temperature oscillation curve. Related to the coating, there is an offset in the temperature oscillation given by ΔT_{film}

$$\Delta T_{total} = \Delta T_{substrate} + \Delta T_{film} . \tag{37}$$

The value of $\Delta T_{substrate}$ is obtained by measuring or calculating the temperature oscillation for the uncoated substrate, while the temperature oscillation ΔT_{total} is obtained from measuring the coated sample. Subtracting those temperature oscillations gives ΔT_{film} which is proportional to the coating thickness t and inverse proportional to the thermal conductivity of the coating K_{film} [24].

$$\Delta T_{film} = \frac{t}{2bl\,K_{film}} . \tag{38}$$

The dimensions of the heater line are given by its width $2b$ and length l.

3.5 High frequency measurements

The main disadvantage of the offset model is that it is restricted to coatings exhibiting a lower thermal conductivity than the substrate. The reason for this limitation is that heat accumulates at the substrate interface in case of high thermal conductive coatings. That would in turn lead to heat wave reflection which would degrade performance data.

For coatings with high thermal conductivity a frequency range has to be chosen in such a way that the thermal penetration depth is smaller than the coating thickness. In other words, the thermal wave should only stay inside the coating, without touching the substrate underneath it as shown in the high frequency region in Figure 3. According to equation 24, the thermal penetration depth decreases with increasing frequency. In addition, the thermal penetration depth depends on the thermal diffusivity D of a material. Figure 5 shows the frequency dependence of the thermal penetration depths for three different materials: glass, silicon and diamond. For example, a penetration depth of 5 µm is related to frequencies of 5 kHz, 500 kHz and 5 MHz for glass, silicon and diamond, respectively. The huge difference in the required excitation frequency is due to the ability of the material to conduct heat. As higher the thermal conductivity of a material as higher a frequency is required.

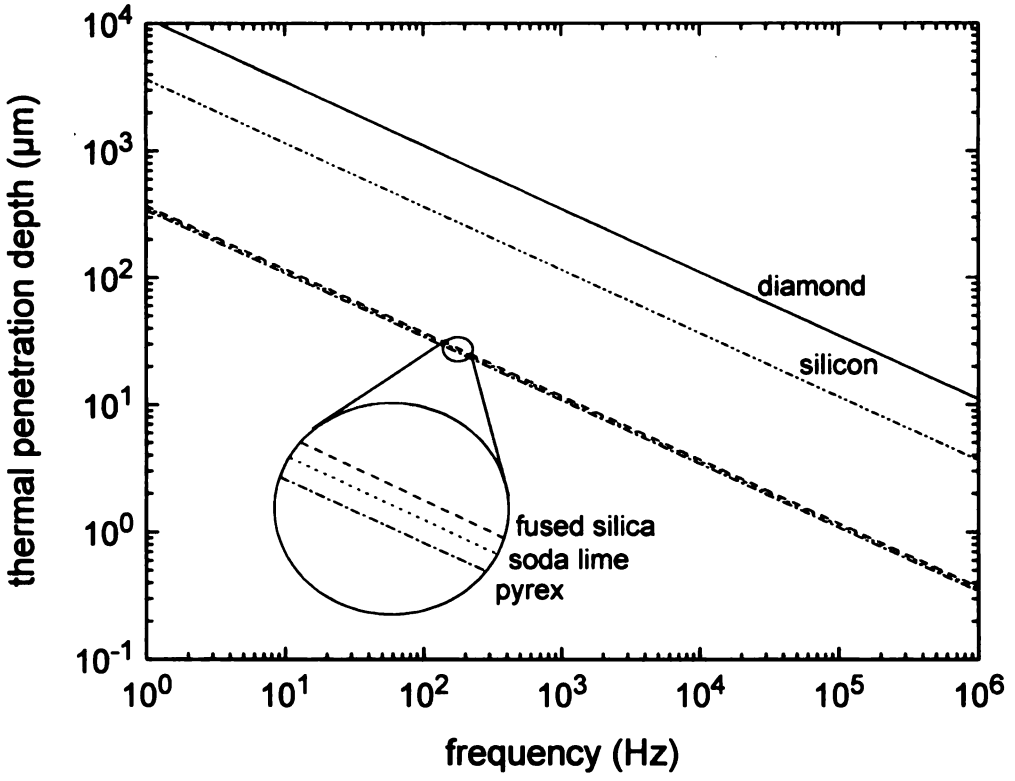

Figure 5. Thermal penetration depth (given in µm) for diamond, silicon and different glass types calculated from equation 24 over a frequency range of 1 Hz to 1 MHz

In case the coating possesses a thickness *t* comparable to or smaller than the heater line width *2b*, the assumption made for low frequency measurements ($q^{-1} >> b$) is no longer valid. Instead of the linear behavior for low frequencies, the measured temperature oscillation for the case $q^{-1} \leq 2b$ asymptotically approaches zero for high frequencies.

When the temperature oscillation versus logarithmic frequency leaves linearity the integral formula (equation 32) has to be used to calculate the thermal conductivity. Writing equation 32 by replacing *q* with equation 24 and 25 gives

$$\Delta T = \frac{P}{l\pi K}\int_0^{\infty} \frac{\sin^2(kb)}{(kb)^2\sqrt{k^2+\left(\frac{i\omega\rho C_p}{K}\right)}}dk \qquad (39)$$

Using MathCAD 2001 and its implemented "fit function" routine, the in-phase or real part of equation 39 can be fitted to the measured temperature oscillation. For the density ρ and the specific heat C_p literature values according to Table 1 are used.

Table 1. Literature values for thermal conductivity *K*, thermal diffusivity *D*, specific heat C_p and thermal expansion coefficient α at room temperature

	K ($W\ m^{-1}K^{-1}$)	D ($10^{-4} m^2/s$)	C_p ($J\ kg^{-1}K^{-1}$)	α ($10^{-6}\ °C^{-1}$)
Diamond I	895 [1]	7.68 [3]	520 [2]	0.11-1.23 [2]
Diamond II a	2300 [1]			
Silicon	148 [1] 141 [2]	0.84 [3]	712 [1]	2.5 [2]
SiO_2	1.5 [1] 1.4 [2]	0.0086 [1]	740 [1]	0.4 [2]
Soda Lime	1.1 [1] 1.7 [2]	0.0081 [1]	840 [2]	9.0 [2]
Pyrex	1.25 [1] 1.4 [2]	0.0074 [1]	850 [1]	3.3 [2]
Silver	429 [1]	1.74 [1]	235 [1]	18.9 [2]
Chromium	94 [1]	0.291 [1]	449 [1]	4.9 [2]

[1] Reference: Lide 2004 [29]

[2] Reference: Callister 2003 [18]

[3] Reference: Leung 1999 [41]

3.6 Electrode design and measurement considerations

The key component of the 3ω measurement system is a thin metal line deposited on a dielectric material. As shown in chapter 3 the metal line functions both, as a heater by carrying electrical current and as thermometer by detecting the change in resistance (which in turn depends on the thermal properties of the coating or substrate material). Four electrode pads are connected to the thin line: two pads function as current leads I^+ and I^- and two pads are the voltage leads V^+ and V^-. The properties of the metal line and the electrode pads have to be optimized to match the 3ω measurement requirements. Also, the dimensions of the metal line and electrode pad assembly should be feasible to be manufactured with reasonable effort.

The metal of the wire and its contacts should have a high thermal conductivity and a low electrical resistance in order to achieve a high electrical power input without increasing the temperature of the metal line significantly. Furthermore, the metal should be chemically inert to ensure reproducible measurements over time. Both factors favor noble metals due to their resistance against reactions with air and their good electrical and thermal properties. A drawback of noble metals is their poor adhesion to most dielectric materials requiring an intermediate adhesion layer.

Table 2 summarizes a literature survey regarding the metal line design and device fabrication.

Table 2. Literature values for the thin metal line parameters including the material, thickness, width and length of the line as well as the patterning method

Line material and thickness	Adhesion layer	Line width	Line length	Patterning method	Reference
Au	Ti	50 μm	10 mm	deposition through a mask	[5]
Ag (500 nm)	Nichrome (10 nm)	5, 35, 90 μm	1 mm	Photolithography, deposition through a mask	[7]
Au	no adhesion layer	10-60 μm	1 mm	N.S.	[16]
Pt (300 nm)	no adhesion layer	90 μm	N.S.*	Photolithography, deposition through a mask	[20]
Au (300 nm)	Cr (3 nm)	25 μm	3 mm	Photolithography	[22]
Au (300 nm)	Cr (2 nm)	8 μm	1 mm	Wet chemical etching	[24]
Al, Cu	no adhesion layer	10, 30 μm	N.S.	Chemical etching process	[25]
Al (200-300 nm)	no adhesion layer	28 μm	4 mm	Chemical etching process	[26]
Ag (150 nm)	no adhesion layer	50 μm	N.S.	N.S.	[27]
Ni (400 nm)	no adhesion layer	20 μm	2 mm	Photolithography	[28]

* N.S. denotes that the line length or patterning method was not specified in the reference

There are three possibilities to fabricate the heater line and the electrode pads on a specimen surface:

I Deposition through a mask

Probably the easiest way to form the metal line and the electrode pads is to deposit an evaporated metal through a mask containing the desired features (Figure 6). Deposition through a mask is preferred for devices having dimensions not smaller than 50 μm.

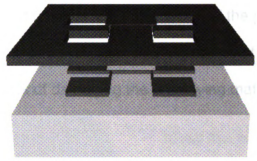

Figure 6. Deposition through a mask: The specimen is covered with a reusable hard mask. Then, the deposition of a thin metal film is performed by evaporation or sputtering.

II Photolithography

Fabricating structures in the nanometer range requires a photolithographic process (Figure 7). First, the entire substrate surface is covered by a thin metal layer that is deposited by metal evaporation or sputter deposition. Second, photoresist patterns are applied using lithography. Those patterns serve as a protection layer for the following etching step, where the metal layer is chemically structured to achieve the final devices. A drawback of the photolithographic process is the difficulty to pattern noble metals because of their high chemical stability as well as the risk of damaging the underlying material.

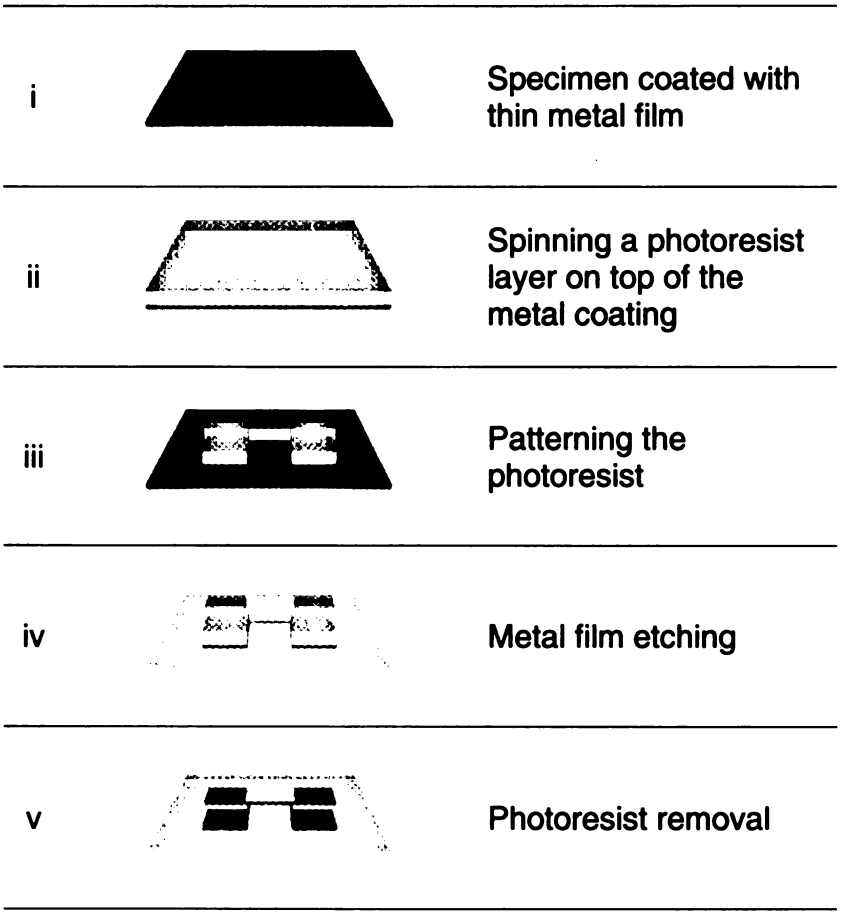

Figure 7. Photolithography: Graphical scheme of the process steps involved in the manufacturing of the electrode device on a sample surface. The device structures are obtained by etching the deposited metal film.

III Lift-off technique

The lift-off technique (Figure 8) overcomes the issues of the photolithographic process by avoiding the etching step and is therefore suitable for almost all substrate materials. Photoresist patterns are supplied to the specimen surface prior to the deposition of the desired metal. When the resist layer is removed by acetone in an ultrasonic bath, the metal is lifted off from those areas that were covered by photoresist, but it remains in the areas that were not protected by the photoresist.

Although this technique is suitable for sensitive substrate materials and for patterning noble metals, the minimum structural dimensions that can be obtained lie in the lower micrometer range.

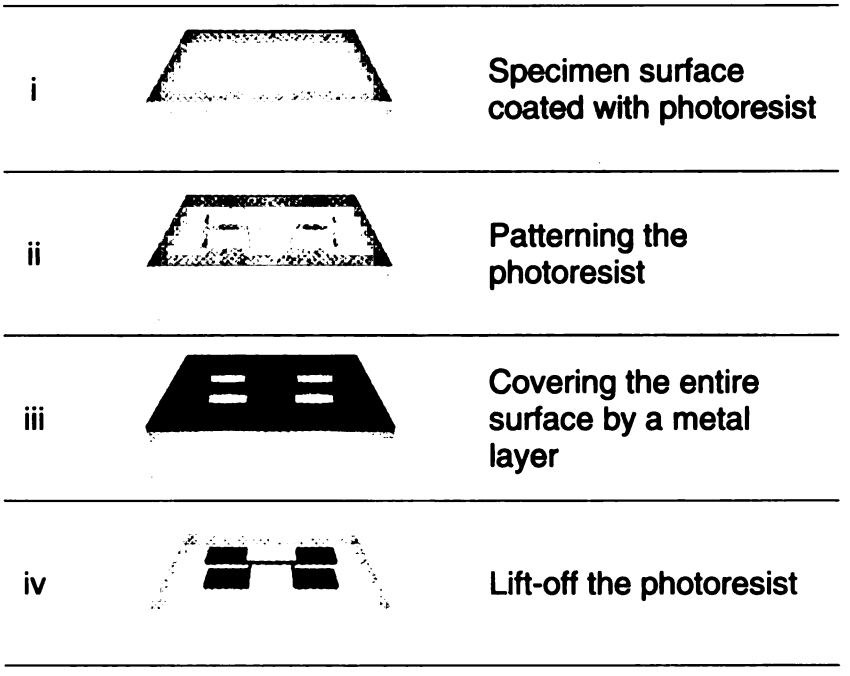

Figure 8. Lift-off technique: Graphical scheme of the process steps to manufacture the electrode device on a sample surface. This process bypasses the metal etching shown in Figure 7.

The geometric aspect of the line length and width is considered by using equation 39. The temperature oscillation, which is directly determined from the 3ω voltage, is proportional to the power input per unit length of the metal line and inversely proportional to the heat conductivity of the underlying material. Most often the power input is limited by the capability of the power supply to deliver a harmonic-free, sine-wave power signal. Those signals are best realizable in the lower power range, which favors shorter lines. On the other hand, the 3ω voltage drop is caused by an electrical resistance modulation at 2ω. The amplitude of the modulation increases with increasing line length. According to the literature, line lengths between 1 and 10 mm are typically used for 3ω measurements. In this study, our goal was to keep the length of the metal line at 1mm.

The role of the line width was discussed in chapter 3. It was shown, that the ratio of the metal line half-width b and the thermal penetration depth q^{-1} defines the curvature of the temperature oscillation plot. As long as the heater line width is much larger than the penetration depth, the temperature oscillation follows a linear line versus logarithmic frequency. When the penetration depth becomes small and comparable to the width of the heater line, the curvature of the temperature oscillation approaches an asymptotic behavior.
In general, as the thickness t of the coating to be analyzed decreases, the metal line width should also decrease. In addition to the frequency dependency, the thermal penetration depth q^{-1} also depends on the thermal diffusivity D (equations 24 and 25).

In materials with a high thermal diffusivity the penetration depth will be high as well. One requirement for measuring by the 3ω method is that the thermal penetration depth is smaller than the film thickness. Figure 5 shows that high frequencies are required for analyzing materials by the 3ω method exhibiting high thermal diffusivities like diamond or silicon. To reach the same thermal penetration depth, glass can be measured with frequencies that are 100 times lower than for measuring silicon and 1000 times lower than for diamond.

To study the influence of the line width on the thermal conductivity measurement of thin films, we decided to use four different line widths: 5 µm, 10 µm, 15 µm and 20 µm.

The final measurement device consisted of metal lines with a length of 1 mm and line widths of 5 µm, 10 µm, 15 µm and 20 µm, which were connected to four electrode pads with an edge length of 1 mm (Figure 9). To fabricate those metal structures on specimens the lift-off technique is used (Figure 8).

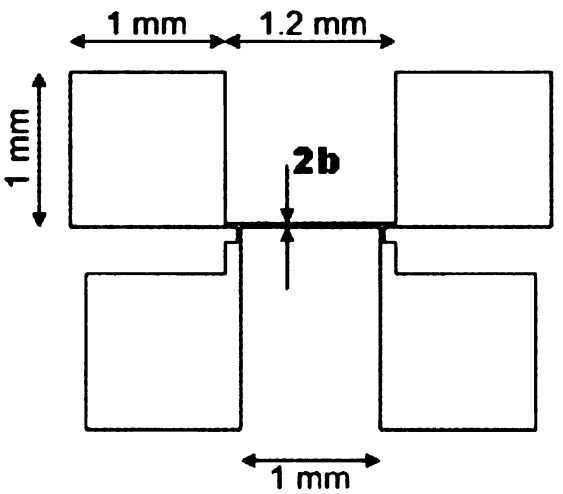

Figure 9. Design and dimensions of an electrode device consisting of the thin metal line of a width *2b* and a length *l* between the lower two pads of 1mm. The electrical connections are realized by four electrode pads each having an edge length of 1 mm^2. Through the upper two pads an alternating current is supplied, while the lower two pads are used for measuring the 3ω voltage.

4 Experimental details

The 3ω measurement can be applied to basically all dielectric materials and films. Required is a sample surface of at least 3 x 4 mm², which is the space needed to supply one electrode device. Besides, a dense and very smooth surface is essential to ensure good adhesion of the metal structure in order to neglect the thermal boundary resistance between metal structures and sample. The experimental of the 3ω method can be divided into three parts:

- The sample preparation which includes deposition the electrode device using a lithographic process for masking and a high vacuum electron beam deposition system for metallization
- Evaluating the temperature coefficient of resistance (*dR/dT*) of the thin metal line by measuring its resistance as a function of temperature
- Measuring the 3ω voltage as a function of excitation frequency

The 3ω method was tested on two different glass samples (Pyrex 7740 and soda lime) and on a bare silicon wafer. Those three samples were supplied with an array of electrode devices consisting of metal lines with different line widths *2b*. On each sample measurements were performed using 4 different line widths: 5, 10, 15 and 20 µm.

To test the 3ω method on thin films, four silicon wafers were thermally oxidized to prepare SiO_2 layers of different thicknesses *t* ranging from 0.3 µm to 3.1 µm. Therefore, silicon wafers were placed into a furnace, which was heated to

typically 800 °C. Oxygen of purity 99.99 % was led through a water bath, whereby the water temperature defined the amount of vaporized water that contributed to the oxidation process in addition to the set amount of oxygen (60 sccm). Detailed information is found in Appendix A, which lists the process parameters and describes the SiO_2 film thickness measurements for the 4 samples used for 3ω measurements.

The 3ω voltage of the silica films were measured using metal line widths of 5 µm, 10 µm and 15 µm for each of the 4 samples.

Figure 10. Photograph of the measurement set-up for the 3ω method with the probe station in the display foreground and the electronic devices in the background

4.1 Sample Preparation

The sample preparation including sample cleaning and supplying the electrodes was carried out in the cleanroom facility at MSU Engineering Research Complex. The manufacturing steps (schematically shown in Figure 8) are based on thin film technologies including mainly masking by lithographic processes and metallization by physical vapor deposition.

A mask consisting of 16 measuring device structures with varying widths of the metal line between the electrodes was manufactured by PhotoSciences, Torrance CA. One measuring device consists of a thin metal line with a length of 1 mm connected to four electrode pads, each having a square area of 1 mm^2. The electrode device is made of a 5 nm chromium layer followed by a 200 nm silver layer, whereby the chromium is functioning as an adhesion layer between the substrate and the silver layer. Silver was chosen as an electrode material because of its high thermal and electrical conductivity. As the metal line works as both heater and thermometer, those properties are essential for measuring thermal conductivity of the underlying film or substrate.

To ensure an optimal contact between sample and measuring device all process fabrication steps have to be carried out with high thoroughness.

4.1.1 Sample cleaning

To remove organic and inorganic residuals on the sample surface, the sample was put in a beaker filled with acetone and cleaned in a commercial ultrasonic bath for 20 min. After rinsing the sample with de-ionized water the sample was placed into a beaker filled with methanol and agitated by ultrasonics for another 20 min. Meanwhile 150 ml isopropanol in a glass beaker was brought to a boiling on a heating plate. After rinsing the sample thoroughly with de-ionized water it was exposed to the isopropanol vapor. The sample was held by a pair of tweezers face down towards the isopropanol. By slightly turning the sample across its axes, it could be visually observed, how the isopropanol vapor carries away all water drops leaving the sample surface clean and water-free. This process was carried out for approximately 5 min. A dehydration bake at 150 °C for 35 min in a furnace (BlueM Stable-Therm® Gravity Oven C-3991-Q) under laboratory air drove off any remaining moisture that might be present on the sample surface.

4.1.2 Lithography

The cleaned substrate was placed on the chuck of the spinner (Laurell Techn. Comp. USA, WS-400B-NPP-Lite). To enhance adhesion between photoresist and substrate hexamethyldisilizane (HMDS 100%, Transene Comp. Inc., Danvers MA) was applied by a disposal pipette in such a way, that it covered the entire sample surface. The sample was fixed on the chuck by vacuum and after applying HMDS rotated with a speed of 3,000 rpm for 30 sec. Due to the spinning the surface was dried and the remaining very thin HMDS layer could react with the ambient air to form reactive silicon hydroxide bonds.

Immediately after rotation stopped, a photo-sensitive polymeric material, called photoresist (Shipley 1813, MicroChem Corp., Newton MA), was applied by a second disposal pipette on the entire sample surface. The same spinning parameters (3,000 rpm and a time of 30 sec) were used to dispense the photoresist across the substrate resulting in a uniform photoresist thickness of 1.2 μm. The photoresist coated sample was then placed into a BlueM furnace and "soft baked" at 80 °C for 20 min under laboratory air to drive off excess solvent before the sample was introduced into the exposure system.

A mask aligner (Karl Suss MJB 3 UV300) was used to expose the photoresist through a chromium coated glass mask. UV light of wavelength between 380 – 500 nm exposes all parts not being shadowed by the chromium-coated mask. The exposure time was set to 30 sec. When the image of the mask is projected onto the sample, the photoresist undergoes wavelength-specific radiation-

sensitive chemical reactions, which cause the regions exposed to light to become more acidic.

During the 30 sec exposure time a beaker large enough for the sample was filled with a photoresist specific developing solution (MF319 developer, MicroChem Corp., Newton MA) to a liquid level of 1 cm. The sample was placed into the developer containing beaker immediately after the UV-light turned off. Exposed acetic photoresist was now soluble in developer solution and was therefore washed away. Photoresist that was shadowed by the mask and not exposed to the UV light is resistant to developing solution and remained on the specimen surface as photoresist patterns.

The developing process can be observed visually by a localized dark red color that arises from the reaction between acetic photoresist and developer. Agitating the beaker slightly by hand leads to a dilution of the red color, revealing if the reaction is still ongoing. After the reaction was completed (approximately 1.5 min) the patterns were absolutely color-free and the sample was taken out of the solution, rinsed for 10 sec with de-ionized water and dried with nitrogen.

The sample is then "hardbaked" in a furnace under laboratory air at 130 °C for 35 min in order to solidify the remaining photoresist pattern.

4.1.3 Metal deposition

Physical vapor deposition (PVD) was used to coat the sample with a thin metal layer. An electron beam vaporized the desired metal in a highly evaporated system (Kurt J. Lesker AXXIS). The sample was fixed using commercial razor blades on the substrate table. The metals chromium (99.998 % pure, 1-6 mm random size chromium pieces, Kurt J. Lesker, Clairton PA) and silver (99.99 % pure, ¼" ø x ¼", Kurt J. Lesker, Clairton PA) were put into graphite crucibles (Kurt J. Lesker, EVCFABEB-23, volume: 3.7 cm^3). After loading the sample and the crucibles, the system was pumped down to a pressure of less than $5 \cdot 10^{-6}$ torr, which took at least 4 hours. Using vacuum level and ultra pure metals ensured a deposited metal film of high quality. After reaching the desired vacuum level, a 5 nm thin chromium layer was deposited. Typical parameters for Cr were a chamber pressure of $1 \cdot 10^{-7}$ torr and an electron beam current of 18 mA leading to a deposition rate of 0.1 nm/s (measured by an implemented piezoelectric transducer). When the 5 nm of Cr were deposited, the electron beam was turned off and held for 20 min to let the melted Cr in the crucible cool down. Then, the rotation stage housing the crucibles was turned to center the silver containing crucible. A 200 nm silver layer was deposited with typical parameters of $1 \cdot 10^{-6}$ Torr for the chamber pressure and 50 mA for the electron beam current leading to a deposition rate of again 0.1 nm/s. A temperature measurement device controlling the substrate holder temperature indicated, that the temperature during deposition remained nearly at room temperature. It never exceeded 27 °C.

4.1.4 Lift-off

After the metal deposition, the entire sample surface was metallized including the surface of the photoresist pattern. By dissolving the photoresist all metal covering the pattern got removed leaving behind only those metal parts, which touch the sample surface directly. Photoresist can be stripped by acetone. Therefore, the sample was placed into a beaker filled with acetone. The lift-off process was enhanced by ultrasonic agitation and carried out until all metal structures were clearly recognizable. Then, the acetone was changed against new acetone solution for a 20 min final cleaning of the sample.

After rinsing thoroughly with de-ionized water and drying with nitrogen, the samples were ready for the thermal conductivity measurements.

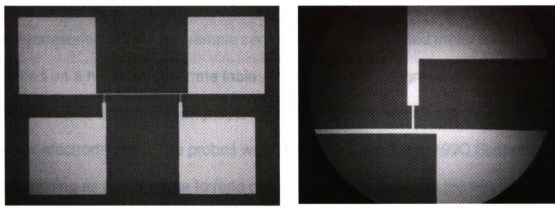

Figure 11. Micrographs of a specimen supplied with 3ω measurement patterns (right: 25x; left: 125x magnification)

4.2 dR/dT measurements

The temperature oscillation is a function of the resistance of the deposited metal strip. In order to calculate the thermal conductivity the resistance versus temperature behavior of the thin metal line has to be measured.

For measuring dR/dT, the sample consisting of the deposited metal pattern was placed on a heatable substrate table, which is part of a Signatone Probe Station (Signatone S-1060 QuieTemp System). Two copper probes were put on the two lower electrode pads. The probes were connected to a Fluke 199C Scopemeter functioning as a multimeter to read out the resistance between the two lower pads. A stable resistance read-out ensures a sufficient contact between the probes and the electrode pads.

The temperature was measured by a Fluke 80T-150U temperature probe placed on the sample surface at a location approximately 5 mm from the electrodes. The temperature was read by a Hewlett Packard Multimeter 34401A. The substrate table was heated with a rate of 2.5 °C/min. Beginning at room temperature up to 150 °C the resistance was recorded every 5 °C. After reaching 150 °C the substrate table heater was turned off. While the sample cooled down, the resistance was again monitored every 5 °C until 50 °C were reached.

At least one more temperature rising procedure was carried out to get sufficient data points for calculating the change of the resistance over temperature. This slope gives the *dR/dT* value for the measured heater line.

4.3 3ω - Measurements

The sample was placed on the chuck of a Janis ST-4LF-2MW-21-CX probe station (Figure 12). Four probes were placed on the device electrodes. The two upper pads were used to supply electrical current of angular frequency by a source generator (Hewlett Packard 8116A Pulse/Function Generator 50MHz), while with the two lower pads the voltage at 3ω was read out. In serial to the electrode device a 15 Ohm resistor was placed.

The signals of the resistor as well as of the device were sent to two differential amplifiers (IC opamp 300 MHz high-speed MAX477EPA). The gain for the amplifier connected to the serial resistor was adjusted in such a way that the 1ω voltage for the resistor and the electrode device were equal. That set-up (schematically shown in Figure 13) was used in order to cancel out the 3ω voltage coming from the source generator.

Then, the signals of those two amplifiers were led to a third differential amplifier, which took the difference of the two incoming signals. The third amplifier was connected to a lock-in amplifier (EG&G Instruments 7265 DSP) giving the voltage at the third harmonic of the thin heater line.

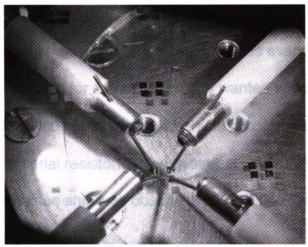

Figure 12. 3ω measurement of soda lime glass: Probing of an electrode device using a Janis Probe Station

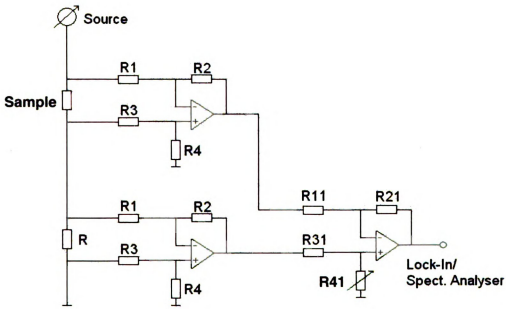

Figure 13. Electronic circuit of the 3ω measurement set-up. All numbered resistors were of equal magnitude R = 320 ohm. The resistor R was adjusted to have the same resistance as the heater line (sample).

Before starting a measurement, the probe chamber was evaporated and the source generator preheated for 1 hour. Then, the wanted voltage was set at the source generator. The value of the 1ω voltage was zeroed by changing the gain of the amplifier of the serial resistor. This adjustment was carried out at 1 kHz and as no change in phase shift was observed up to 300 kHz it was valid for the entire frequency range.

The readout of the lock-in amplifier was changed to give the voltage at 3ω for the metal line directly. Starting at low frequencies the set point of the frequency at the source generator was logarithmically increased up to 80 kHz and the corresponding 3ω voltage was recorded.

As the lock-in amplifier was only capable for frequencies up to 250 kHz, which would correspond to read out 3ω values up to a third of 250 kHz, a spectrum analyzer (Tectronic 2754P) was used for measuring 3ω voltage from 50 kHz to 300 kHz. The overlapping range of the lock-in amplifier and the spectrum analyzer between 50 kHz and 80 kHz could be used to control the accuracy and reproducibility of our data.

5 Results and discussion

Initial tests of the experimental apparatus were performed on bulk materials that model a one-layer system with infinite sample thickness. This assumption is necessary for using one dimensional heat flow calculations (chapter 3.1), which neglects heat wave reflections from the rear surface of the sample. Two glass materials, soda lime and Pyrex, were chosen, because of their low thermal conductivity values. In an extension of the 3ω method to higher thermal conductivities, silicon was measured, which is approximately two orders of magnitude more conductive than glass. A wide frequency range was used to record the 3ω voltage, which allowed the data to be analyzed by the slope model for lower frequencies (chapter 3.2) as well as the fit method for the entire frequency range (chapter 3.5).

In addition, two-layer systems consisting of thin silicon dioxide films on silicon were investigated. As the thickness t of the silica films was smaller than the metal line widths $2b$, the slope model for determining thermal conductivity was no longer valid. Instead, the offset-model for the low frequency range was compared to the fit method for high frequencies.

5.1 Measurements on bulk materials

Two glass wafers (soda lime and Pyrex) and one silicon wafer were equipped with 3ω measurement patterns using the lift-off technique (as described in section 4.1. The patterns consisted of heater lines, where the width *2b* was 5 µm, 10 µm, 15 µm and 20 µm (Figure 14). One device of each line width was used on a given sample resulting in four thermal conductivity measurements on one sample.

First, the heater line was calibrated. By recording and differentiating the resistance of the metal line as a function of temperature, one determines the resistance change per unit of temperature difference. This value, also referred to as *dR/dT*, is assumed to be constant over the temperature range of interest. Dividing the *dR/dT* value by the resistance of the metal line at 20 °C gives α, the relative change of resistance versus temperature.

In Table 3 the values of α determined for the bulk material measurements are listed. Thee mean value of α is (0.0033 ± 0.0004) K^{-1}. In order to reduce the measurement error, α values were recorded for each metal line instead of using the mean value.

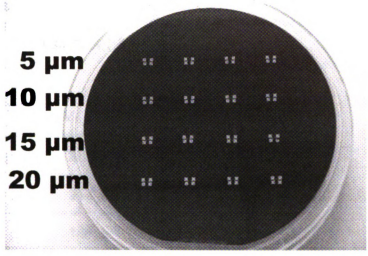

Figure 14. Silicon wafer supplied with an array of metal patterns. For each row values for the metal line widths *2b* are indicated on the left side of this figure.

Table 3. Electrical and thermal parameters and their standard deviations for the 3ω measurements of Pyrex 7740, soda lime, and silicon. These parameters were subsequently used to determine the thermal conductivities at varying line widths *2b*. From the voltage drop $V_{1\omega}$, measured parallel to the voltage pads, and the current across the line measured in series (not shown in the table), the power per unit length *P/l* is calculated. To determine the temperature *T* of the specimen, the resistance of the metal line is measured twice: first with a small voltage to avoid heating of the sample and the second time with a voltage $V_{1\omega}$ used for 3ω measurements. By knowing the temperature coefficient of the resistance α, the temperature *T* of the sample during measurement can be determined.

	Line width	$V_{1\omega}$ (mV)	P/l (W/m)	α (K^{-1})	T (°C)
Pyrex 7740	5 μm	365 ± 1	4.34 ± 0.05	0.0038 ± 0.0001	33 ± 2
	10 μm	217 ± 1	3.13 ± 0.04	0.0035 ± 0.0001	27 ± 1
	15 μm	186 ± 1	3.01 ± 0.03	0.0034 ± 0.0001	28 ± 1
	20 μm	256 ± 1	2.85 ± 0.04	0.0028 ± 0.0001	31 ± 2
Soda Lime	5 μm	364 ± 1	3.67 ± 0.05	0.0037 ± 0.0001	31 ± 1
	10 μm	278 ± 1	3.89 ± 0.04	0.0033 ± 0.0001	42 ± 2
	15 μm	208 ± 1	3.42 ± 0.04	0.0034 ± 0.0001	36 ± 2
	20 μm	169 ± 1	2.94 ± 0.03	0.0035 ± 0.001	38 ± 2
Silicon	5 μm	1159 ± 1	49.6 ± 0.3	0.0028 ± 0.0001	33 ± 1
	10 μm	795 ± 1	45.1 ± 0.2	0.0032 ± 0.0001	27 ± 1
	15 μm	650 ± 1	38.9 ± 0.2	0.0030 ± 0.0001	28 ± 1
	20 μm	846 ± 1	46.2 ± 0.2	0.0023 ± 0.0001	31 ± 1

During the 3ω measurements the input voltage was adjusted so that the resulting 3ω voltage was between 1 and 3 mV at lower frequencies. This voltage range is sufficient to achieve stable read-outs on the one hand and to avoid an overheating of the thin metal line on the other hand. By measuring the 1ω voltage and current, the input power and the actual resistance of the metal line was calculated. Using the resistance of the heater line and the input power, the sample temperature was then determined (see Table 3).

Due to the difference between the thermal conductivities of glass and silicon, silicon required much higher input powers to achieve similar 3ω voltages. Since silicon is a better thermal conductor than glass, those high input powers did not increase the sample temperature. In general, sample temperatures were determined to be slightly above room temperature at 27 – 43 °C.

Figure 15 and Figure 16 show the measured 3ω voltage as a function of logarithmic frequency for Pyrex and soda lime, respectively. Both glass samples were 1 mm thick and were measured using input voltages with frequencies between 1 Hz and 100 kHz. According to the damping distance of the thermal wave (equation 24), this frequency range is equivalent to a probing depth of approximately 350 μm to 1 μm. Since the maximum penetration depth of 350 μm is smaller than the sample thickness of 1 mm, the assumption of neglecting heat wave reflection from the sample backside is reasonable.

For the silicon sample, which was 350 μm thick, thermal conductivity measurements were made at a frequency range of 200 Hz to 10 kHz (Figure 17), which is equivalent to a probing depth of about 260 μm to 35 μm.

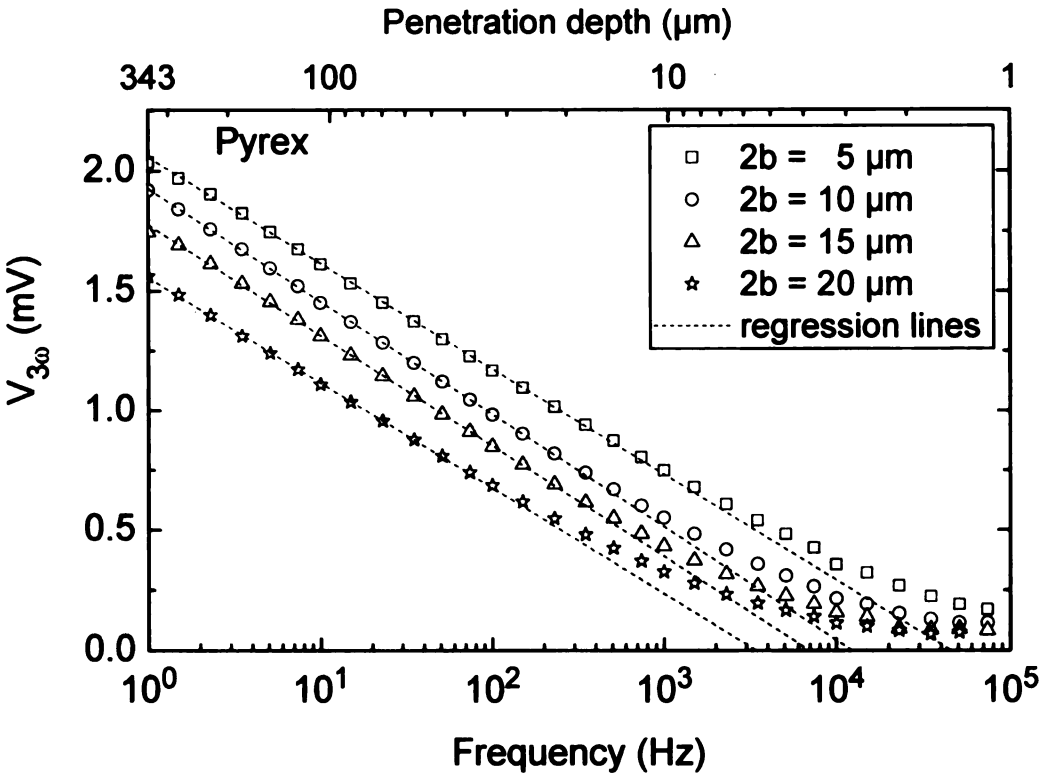

Figure 15. Plot of the measured 3ω voltage for Pyrex 7740 at varying metal line widths *2b*. A linear regression was performed for frequencies below 200 Hz to determine the thermal conductivity by the slope method, which gave a mean value of K = 1.3 W/(m·K). (For better clarity, only every third data point is included in the plot.)

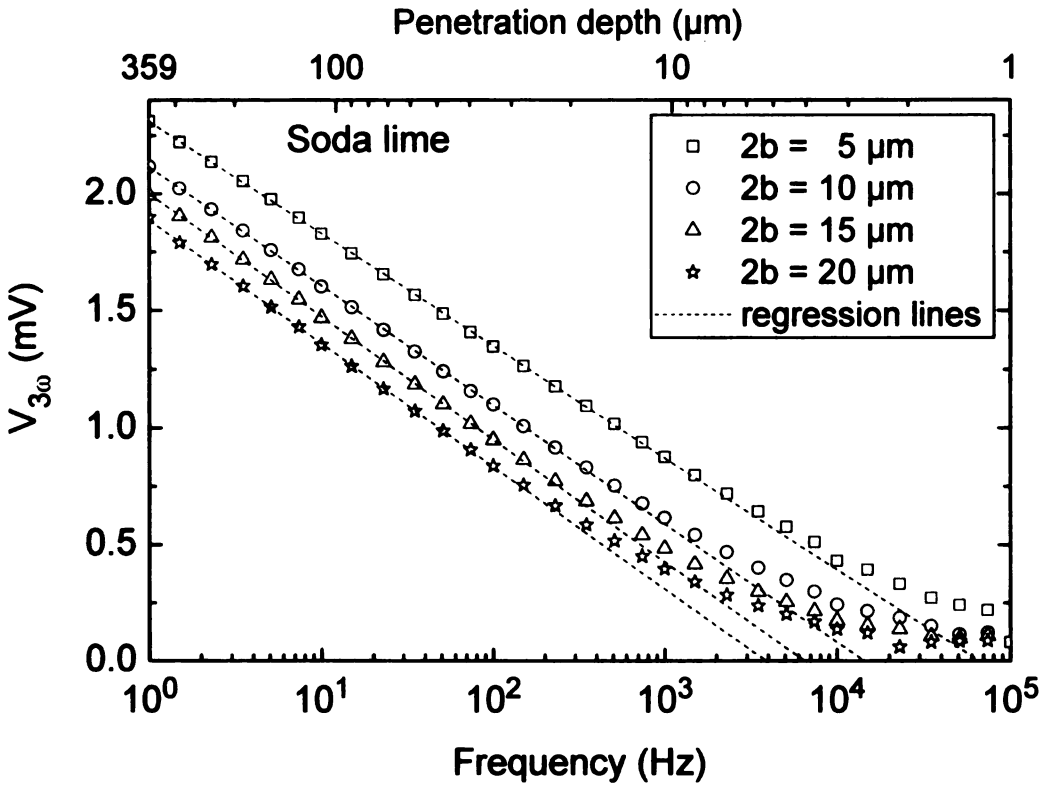

Figure 16. Plot of the measured 3ω voltage for soda lime at varying metal line widths *2b*. A linear regression was performed for frequencies below 200 Hz to determine the thermal conductivity by the slope method, which gave a mean value of K = 1.1 W/(m·K). (For better clarity, only every third data point is included in this plot)

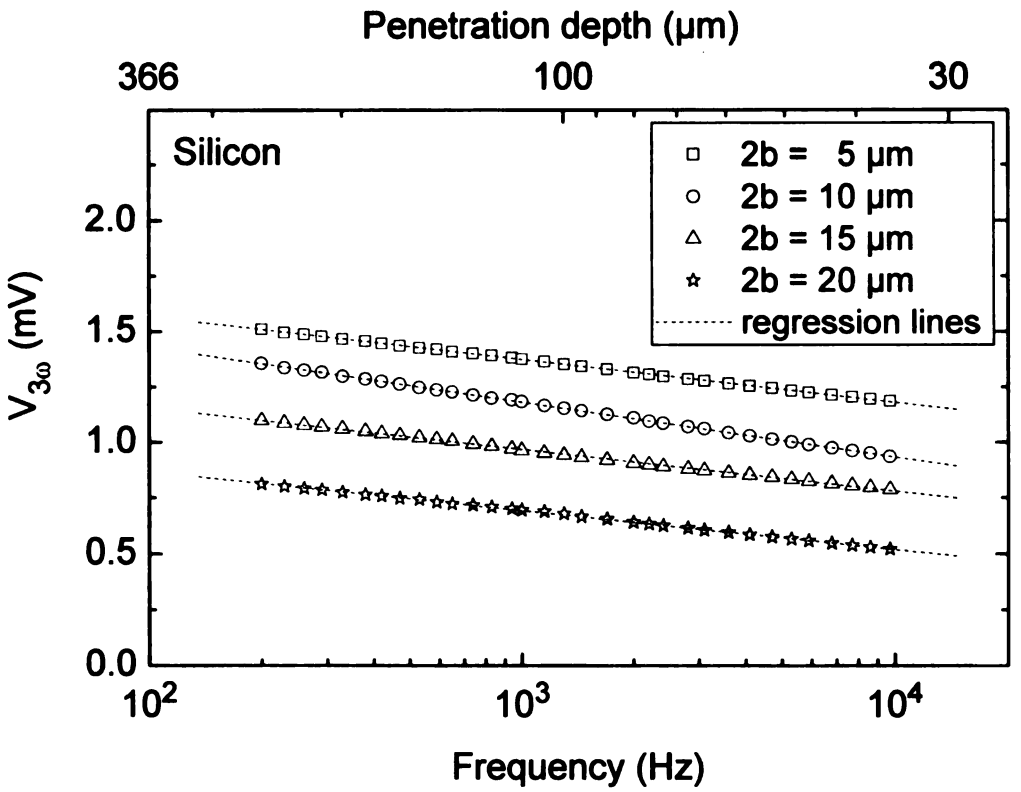

Figure 17. Graphs of the 3ω voltage for silicon measured between 200 Hz and 10 kHz. The plotted graphs were taken from one silicon wafer that was equipped with an array of electrode devices with varying line widths *2b*. A logarithmic regression of the form y = m·ln(x)+n was performed (plotted by black solid lines) to determine the thermal conductivity with equation 34. The thermal conductivity values are included in Table 4.

From the 3ω data (Figure 15, Figure 16, Figure 17) the lower frequency data was included in a logarithmic regression to determine the thermal conductivity *K* by the slope model (section 3.2). The thermal conductivity is inversely proportional to the slope of the logarithmic regression line (equation 34). The higher slopes in the 3ω plots of the soda lime and Pyrex sample indicate a lower thermal conductivity than the lower slope observed for the silicon sample (Figure 17).

For the silicon sample, the 3ω voltage follows a straight line over the entire measured frequency range (on a logarithmic scale), allowing one to use frequencies up to 10 kHz for the slope model. For the glass samples, the frequency at which the 3ω voltage departs from linearity depends on the metal line width *2b*. For a line width of 5 μm the upper frequency limit is about 1 kHz, while for a 20 μm wide line, this limit is reached at about 200 Hz. This confirms that the linear range of the temperature oscillation is extended to higher frequencies by using a thinner line width *2b*.

In a second step, the application of the slope model was compared to the fit model. Using equation 20, the 3ω voltage was converted to a temperature oscillation. The resulting temperature oscillation plots for Pyrex, soda lime and silicon were fitted to equation 34 to determine the thermal conductivity values, *K*, (Figure 18, Figure 19 and Figure 20). The measured and fitted data agree well over the entire frequency range for both the thermally low conductive glass materials possessing a non-linear behavior of the temperature oscillation as a function of the logarithmic frequency (Figure 18, Figure 19), as well as the higher thermal conductive silicon with its linear temperature oscillation (Figure 20).

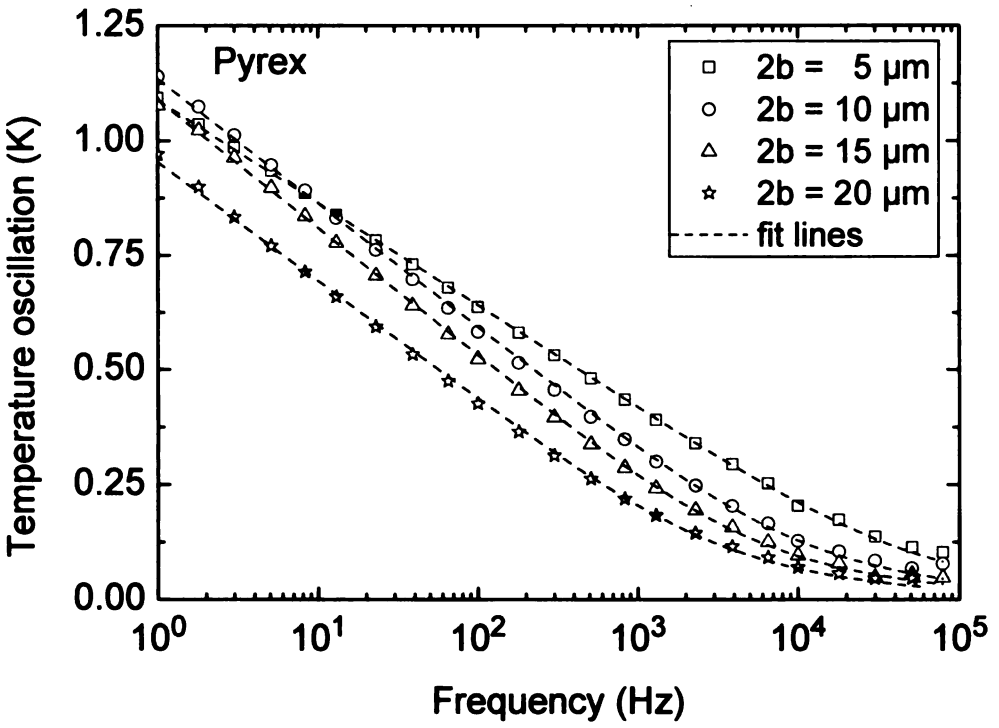

Figure 18. Fit model applied to 3ω measurements of Pyrex. The temperature oscillation, which is measured with different heater line widths *2b*, is plotted as a function of frequency for soda lime and fitted to equation 39. The fitting plots for each line width are represented by dotted lines. In comparison to Figure 15 the entire frequency range can be used for data fitting. (For better clarity, only every fourth data point is included in this plot.)

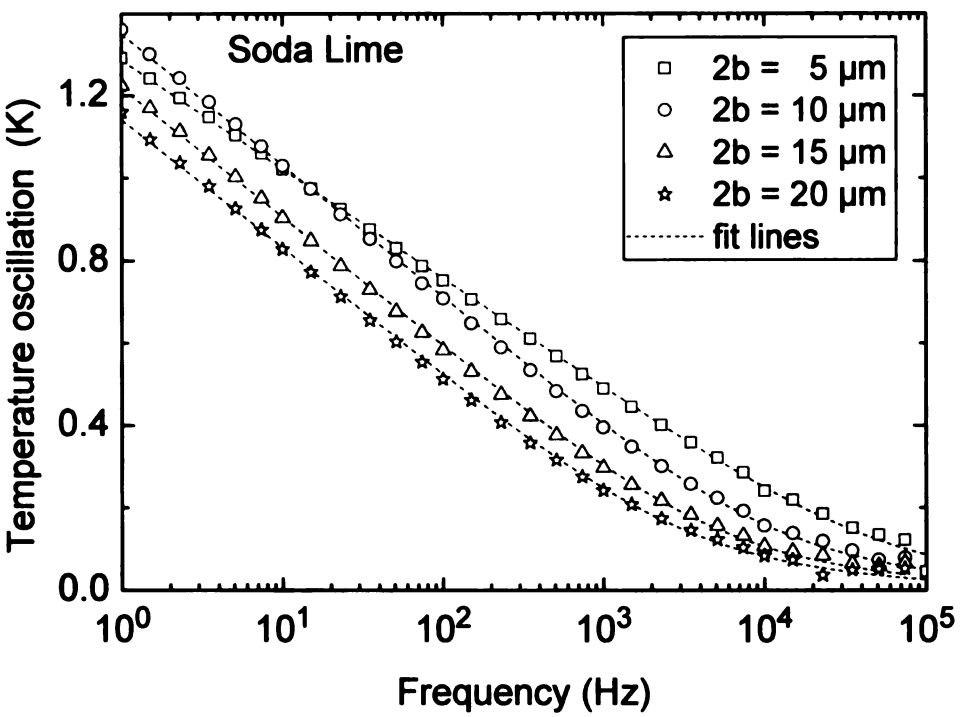

Figure 19. Fit model applied to 3ω measurements of soda lime. The temperature oscillation, which is measured with different heater line widths *2b*, is plotted as a function of frequency for soda lime and fitted to equation 39. The fitting plots for each line width are represented by dotted lines. In comparison to Figure 16 the entire frequency range can be used for data fitting. (For better clarity, only every fourth data point is included in this plot.)

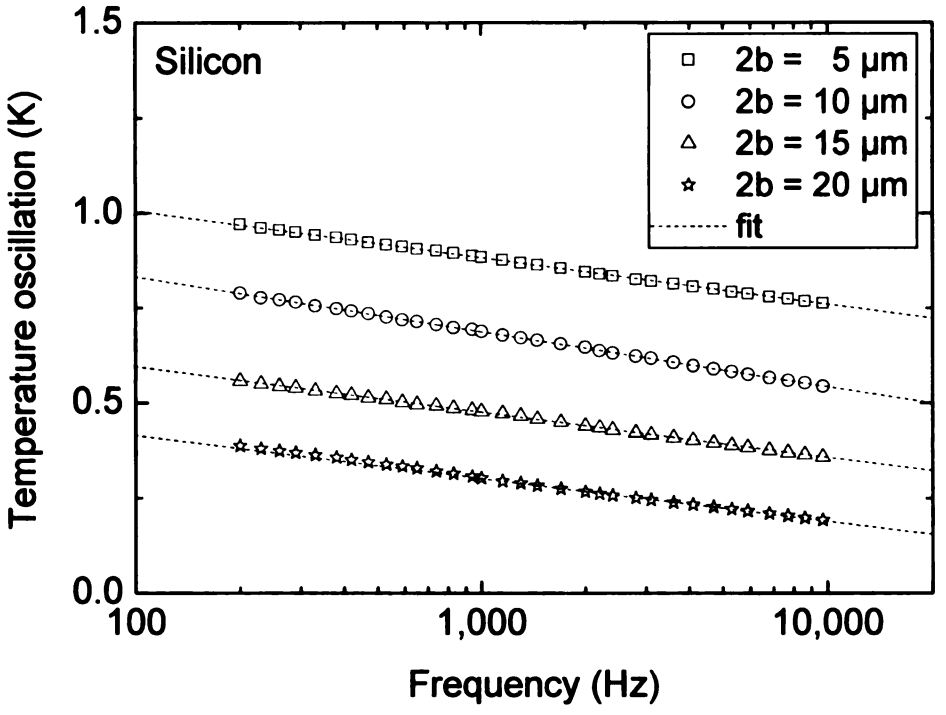

Figure 20. Graphs of the temperature oscillation for silicon determined from the data shown in Figure 17 and equation 20. The plotted data were fitted to equation 39 to determine the thermal conductivity of silicon. The thermal conductivity values are included in Table 4.

Table 4 summarizes the thermal conductivity values determined by the slope and fit method are summarized showing the determined thermal conductivities for the four different line widths investigated for Pyrex, soda lime and silicon. Both the slope and the fit method show only minor deviations in the resulting thermal conductivities *K* of the same sample. However, the thermal conductivities calculated using a line width of 5 μm is slightly higher than the average value for each of the specimens. In general, soda lime has the lowest thermal conductivity value of 1.13 W/(m K) for the slope method and 1.17 W/(m K) for the fit method. Both values agree well with reference values for soda lime of K = 1.1 W/(m K) [29]. Pyrex possesses a slightly higher thermal conductivity (1.31 $W(m\ K)^{-1}$) as determined by the slope method compared to 1.36 W/(m K) determined from the fit method. Reference values for the thermal conductivity of Pyrex range from 1.25 W/(m K) [29] to 1.4 W/(m K) [18], which agrees well with the thermal conductivity values determined in this study. The observed thermal conductivities for silicon of 131 W/(m K) for the slope method and 130 W/(m K) for the fit method are only slightly below reference values of 141 W/(m K) [18] and 148 W/(m K) [29]. For silicon, the difference between the literature values and the values determined in this study might be caused by the doping level of the silicon specimen that was measured in our study. Doping can cause an increased phonon scattering by impurity atoms resulting in a lower thermal conductivity value [12].

Table 4. Comparison of the thermal conductivities *K* calculated by the slope method (equation 34) and fit method (equation 39) for Pyrex 7740, soda lime, and silicon for different heater line widths *2b*. The given uncertainties are calculated by the error extension law by using the values of Table 3 and an additional 2% error for the line width *2b* for the fit method. The coefficient of determination R^2 measures how well the data are described by the regression or fitting curve. R^2 makes no conclusions about the error of the thermal conductivity.

Line width		Slope method		Fit method	
		K (W $m^{-1}K^{-1}$)	R^2	K (W $m^{-1}K^{-1}$)	R^2
Pyrex 7740	5 µm	1.48 ± 0.09	0.9997	1.64 ± 0.08	0.9989
	10 µm	1.31 ± 0.07	0.9999	1.35 ± 0.08	0.9994
	15 µm	1.29 ± 0.08	0.9994	1.31 ± 0.09	0.9996
	20 µm	1.33 ± 0.09	0.9997	1.41 ± 0.11	0.9990
	average	**1.31 ± 0.02**		**1.36 ± 0.05**	
Soda Lime	5 µm	1.37 ± 0.07	0.9999	1.39 ± 0.09	0.9989
	10 µm	1.12 ± 0.06	0.9999	1.15 ± 0.08	0.9990
	15 µm	1.13 ± 0.06	0.9999	1.17 ± 0.08	0.9995
	20 µm	1.14 ± 0.07	0.9998	1.18 ± 0.08	0.9913
	average	**1.13 ± 0.01**		**1.17 ± 0.02**	
Silicon	5 µm	146 ± 6	0.9997	139 ± 8	0.9983
	10 µm	115 ± 3	0.9999	114 ± 5	0.9997
	15 µm	119 ± 4	0.9995	116 ± 6	0.9986
	20 µm	144 ± 4	0.9988	150 ± 7	0.9994
	average	**131 ± 16**		**130 ± 18**	

5.2 Measurements of silica films on silicon

Four silicon wafers were oxidized to create thin SiO_2 films of different thicknesses *t* varying from 0.3 to 3.2 μm. Table 5 shows the parameters used for thermal oxidation and the resulting film thicknesses measured by a laser acoustic wave method (for further details please see Appendix A).

Each sample was supplied with metal patterns of line widths 5, 10 and 15 μm. The 3ω voltage was measured in a frequency range of 500 Hz to 300 kHz. Values for the power supplied to the metal line, the resulting sample temperature and the temperature coefficient of the metal line's resistance (determined prior to the 3ω measurements) are included in Table 6. The input power for measuring thicker SiO_2 films was comparable to the input power used to measure the glass samples. For the thinnest film of 0.3 μm, a power input level similar to that used for pure silicon was necessary. The mean temperature coefficient of the heater line's resistance is $0.0037 \pm 0.0003\ K^{-1}$. Again, the sample temperature during 3ω measurements was slightly above room temperature at 25 – 35 °C.

Table 5. Matrix of the process parameters used to prepare silicon dioxide films on silicon by thermal oxidation

Sample	Furnace temperature	Water temperature	Oxidation time	SiO_2 Film thickness
1	800 °C	22 °C	4 hrs	0.3 μm
2	800 °C	76 °C	19 hrs	1.2 μm
3	800 °C	76 °C	52 hrs	2.3 μm
4	1000 °C	76 °C	77 hrs	3.2 μm

Table 6. Electrical and thermal parameters and their standard deviations for the 3ω measurements of silicon dioxide films on silicon. These parameters were subsequently used to determine the thermal conductivities at varying line widths *2b*. From the voltage drop $V_{1\omega}$, measured parallel to the voltage pads, and the current across the line measured in series (not shown in the table), the power per unit length *P/l* is calculated. To determine the temperature *T* of the specimen, the resistance of the metal line is measured twice: first with a small voltage to avoid heating of the sample and the second time with a voltage $V_{1\omega}$ used for 3ω measurements. By knowing the temperature coefficient of the resistance α, the temperature *T* of the sample during measurement can be determined.

Line width	Film thickness	$V_{1\omega}$ (mV)	P/l (W/m)	α (K^{-1})	T (°C)
5 μm	0.3 μm	903 ± 1	29.9 ± 0.1	0.0034 ± 0.0001	32 ± 1
	1.2 μm	601 ± 1	12.9 ± 0.1	0.0037 ± 0.0001	26 ± 1
	2.3 μm	533 ± 1	7.6 ± 0.1	0.0042 ± 0.0001	25 ± 1
	3.2 μm	524 ± 1	8.6 ± 0.1	0.0036 ± 0.0002	25 ± 2
10 μm	0.3 μm	776 ± 1	37.8 ± 0.1	0.0033 ± 0.0002	32 ± 2
	1.2 μm	721 ± 1	27.0 ± 0.1	0.0037 ± 0.0001	34 ± 1
	2.3 μm	515 ± 1	14.5 ± 0.1	0.0041 ± 0.0001	29 ± 1
	3.2 μm	550 ± 1	16.5 ± 0.1	0.0037 ± 0.0001	34 ± 1
15 μm	0.3 μm	733 ± 1	43.1 ± 0.1	0.0035 ± 0.0001	32 ± 1
	1.2 μm	698 ± 1	37.0 ± 0.1	0.0037 ± 0.0001	33 ± 1
	2.3 μm	586 ± 1	21.0 ± 0.1	0.0036 ± 0.0001	32 ± 1
	3.2 μm	557 ± 1	21.5 ± 0.1	0.0036 ± 0.0001	35 ± 1

Figure 21, Figure 22 and Figure 23 show the resulting temperature oscillation for films measured with the same heater line width *2b*. All three plots show the general curvature of a two-layer system, where the top layer exhibits a lower thermal conductivity than the substrate. Starting at high frequencies the damping distance of the thermal wave is short preventing the heat to diffuse into the silicon substrate. The measured 3ω voltage due to the silica layer is not influenced by the thermal properties of the silicon because the silicon does not "see" the heat wave supplied by the thin metal line. Therefore, the curvature of the temperature oscillation plots for high frequencies appears to be similar to the curvature of the plots for the glass samples. When the frequency gets low enough for the thermal wave to penetrate the entire SiO_2 film into the silicon substrate, the temperature oscillation follows the flat curvature of uncoated silicon. However, it is shifted by an offset ΔT_{film} that is a function of the film thickness *t* and the film's thermal conductivity. By applying the offset model (section 3.4) and equation 38 the thermal conductivities of the four thin film samples were determined, along with the dependence on the line width *2b* (Table 7). Thus, the thermal conductivity is independent of the film thickness *t*, but there seems to be an influence of the line width, since the values of the thermal conductivity decrease slightly with increasing line width. According to Lee [24] the reason might be that the offset model assumes one-dimensional heat flow requiring a heater width *2b* much greater than the film thickness *t*. In our case we might have reached the limit of this assumption by using line widths *2b* comparable to the film thicknesses *t*. Despite these small deviations, the offset

model gives an average thermal conductivity of 1.55 W/(m K) for the silica films on silicon, which agrees well with reference values of 1.4 – 1.5 W/(m K) [18, 29]. The thermal conductivity value obtained by the offset method could be confirmed by fitting the upper frequency region contributing solely to the SiO_2 layers to equation 39 yielding in a mean thermal conductivity of 1.6 W/(m K) (see Table 7). The fit method can be applied only to the thickest silica layer of 3.2 µm. No unambiguous solution was found by trying to fit films thinner than 3.2 µm. However, the fit curvature appears to fit the thinner films visibly.

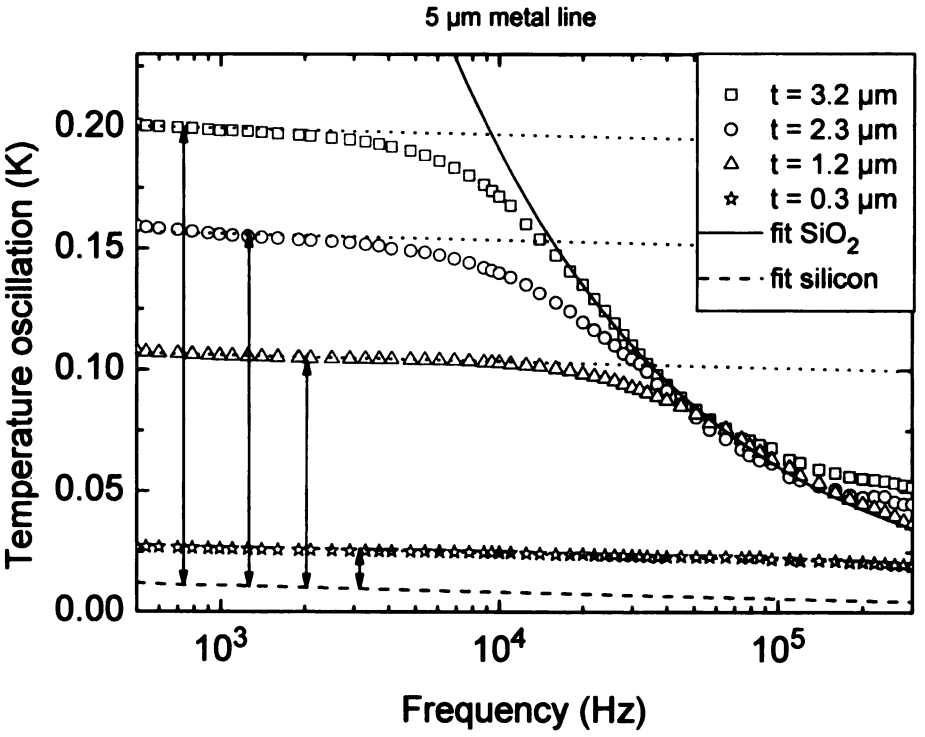

Figure 21. Plot of the temperature oscillation (power normalized) for silicon dioxide films of thickness *t* measured with a 5 μm wide heater line.

The low frequency region is affected by the silicon substrate. Thus, the offset-model can be applied by using the temperature oscillation offset ΔT_{film} (denoted by arrows). The data for higher frequencies includes contributions only from the SiO_2 films and is used to fit measured data to equation 39 (solid line).

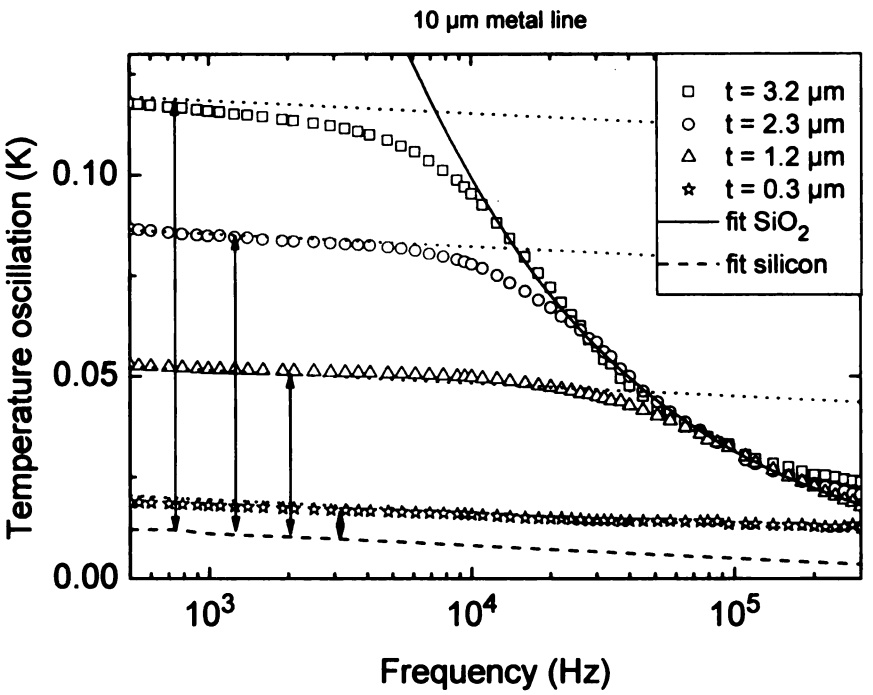

Figure 22. Plot of the temperature oscillation (power normalized) for silicon dioxide films of thickness *t* measured with a 10 µm wide heater line.

The low frequency region is affected by the silicon substrate. Thus, the offset-model can be applied by using the temperature oscillation offset ΔT_{film} (denoted by arrows). The data for higher frequencies includes contributions only from the SiO_2 films and is used to fit measured data to equation 39 (solid line).

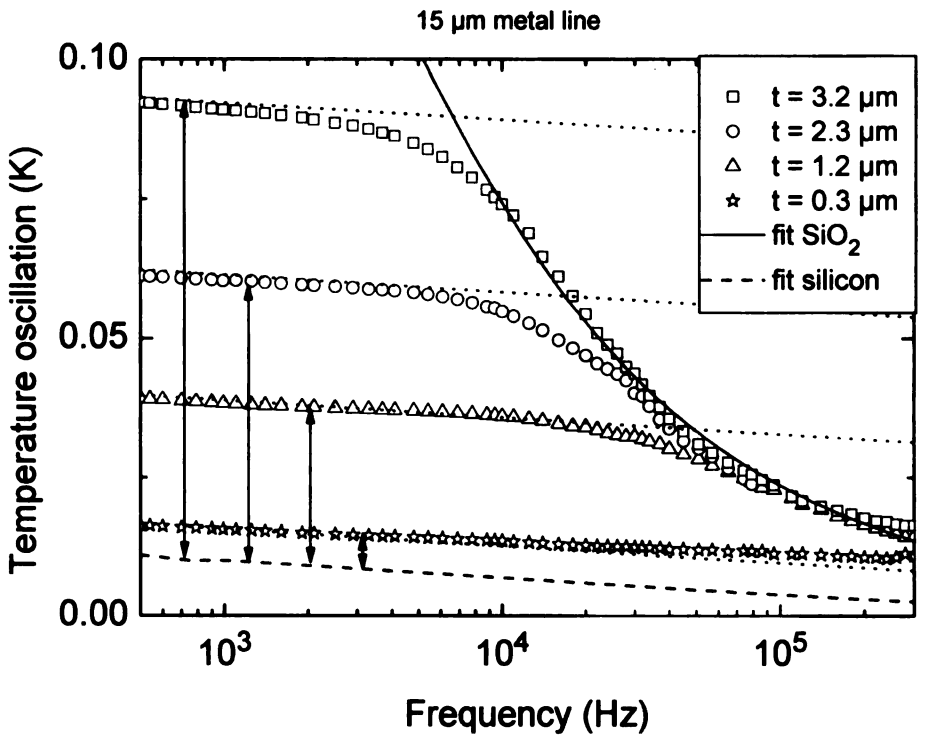

Figure 23. Plot of the temperature oscillation (power normalized) for silicon dioxide films of thickness *t* measured with a 15 µm wide heater line.

The low frequency region is affected by the silicon substrate. Thus, the offset-model can be applied by using the temperature oscillation offset ΔT_{film} (denoted by arrows). The data for higher frequencies includes contributions only from the SiO_2 films and is used to fit measured data to equation 39 (solid line).

Table 7. Comparison of the thermal conductivities *K* determined by the slope method (equation 34) and fit method (equation 39) for silica layers of different thicknesses *t* measured with a series of heater line widths *2b*.

Line width	Film thickness	Offset method	Fit method	
		K ($W m^{-1}K^{-1}$)	K ($W m^{-1}K^{-1}$)	R^2
5 µm	0.3 µm	1. 7 ± 0.2		
	1.2 µm	1.5 ± 0.2		
	2.3 µm	1.6 ± 0.2		
	3.2 µm	1.7 ± 0.4		
	average	**1.63 ± 0.15**	**1.43**	**0.999**
10 µm	0.3 µm	1. 7 ± 0.2		
	1.2 µm	1. 5 ± 0.2		
	2.3 µm	1. 6 ± 0.2		
	3.2 µm	1. 5 ± 0.2		
	average	**1.58 ± 0.14**	**1.56**	**0.992**
15 µm	0.3 µm	1. 6 ± 0.2		
	1.2 µm	1. 4 ± 0.2		
	2.3 µm	1. 5 ± 0.2		
	3.2 µm	1. 3 ± 0.2		
	average	**1.45 ± 0.18**	**1.78**	**0.990**

5.3 Application of the 3ω method for thin diamond films

Materials that are able to dissipate excess heat are of great interest especially for the integrated circuit industry. Diamond, possessing an outstanding thermal conductivity of up to 2300 W/(m K) at room temperature, has gained special attention since scientists and engineers developed techniques to manufacture artificial diamond [30, 31]. Depending on the method, diamond can be fabricated in form of single crystals by a HPHT process (high pressure high temperature) or diamond can be deposited in form of thin films by CVD techniques (chemical vapor deposition), whereby films exhibit grain sizes ranging from hundreds of microns down to a few nanometers.

The thermal conductivity of primary single diamond crystals and free standing polycrystalline membranes has been measured by heated bar and laser flash techniques [8, 10, 32, 33, 34, 35, 36, 37]. In addition, the 3ω method has been used to measure natural or isotropically enriched diamonds [27, 38, 39]. A broad spread of room temperature thermal conductivity values can be found in the literature, ranging from 2265 W/(m K) for natural diamond [34] to the probably highest reported value of 3320 W/(m K) for isotropically enriched ^{12}C diamond [36]. For polycrystalline diamond films, the literature data ranges from 140 W/(m K) for 100 µm grain size [10], to 700 W/(m K) for a grain size of 2 µm [40] and 320 W/(m K) for 150 nm grains [32].

An undeniable dependency between thermal conductivity and grain size of diamond films exists. Since grain boundaries are areas with a high concentration

of lattice distortions, phonons experience a resistance at grain boundaries, when travelling through a crystalline solid. This thermal resistance increases with an increasing number and area of grain boundaries (i.e. smaller grain sizes). That is why, the thermal conductivity of diamond films is expected to decrease with smaller grain size.

As a next step, it would be an interesting challenge to investigate the relationship between grain size and thermal conductivity of diamond films by the 3ω method.

6 Summary and Conclusion

A measurement method to determine the thermal conductivity based on the four-wire 3ω technique was successfully built up. An experimental apparatus was assembled from a commercial probe station and differential amplifiers. Samples were supplied with a thin metal structure using a lithographic process for masking and a high vacuum electron beam deposition system for metallization. The final patterns made of a chromium silver double-layer consisted of a thin metal line functioning both as heater and thermometer and four electrode pads for contacting.

By supplying a current of angular frequency to the heater line, a thermal wave is created which diffuses into the underlying material. The damping distance (or penetration depth q^{-1}) of the thermal wave is a function of the excitation frequency and the thermal conductivity of the sample.

The parameter q^{-1} defines the probing depth, which should always be smaller than the sample thickness t.

Related to the thermal penetration depth q^{-1}, the sample thickness t and the heater width $2b$, different approaches to extract the thermal conductivity from measurement data were tested.

The data analysis included the slope model for thick samples explored by Cahill and co-workers. The slope model is valid as long as the sample thickness is much larger than the heater line width. In this case, the temperature oscillation

versus logarithmic frequency can be approximated by a linear function. In general, the slope model is used to measure the thermal conductivity of uncoated bulk materials.

The thermal conductivity of very thin coatings can be calculated by the offset model. To use the offset model, the film thickness has to be small compared to the heater line width. In addition, the thermal conductivity of the coating must be much smaller than the thermal conductivity of the substrate.

The main drawback of the slope model and offset model is their restrictions to either very thick or very thin films, respectively. In the medium range, where coatings exhibit thickness values comparable to the width of the heater line, the thermal conductivity cannot be calculated with those models.

To fill that medium range, calculating thermal conductivities by the integral formula was introduced. The integral formula can be applied to thin films exhibiting a thickness of a few micrometers and is not limited by a maximum film thickness. In contrast to the offset model, the integral formula is not restricted to films of low thermal conductivity values.

7 Outlook

The 3ω method was successfully extended to high frequencies of up to 300 kHz by assembling an experimental apparatus. Re-designing that apparatus by decreasing the size of the probing station and drastically decreasing the length of the cables that are directly connected to the electrode device can help to further extend the frequency range. Especially for measuring materials with a high thermal conductivity, measurements under vacuum and temperature stabilization are suggested to enhance the stability and reproducibility of the recorded 3ω voltages.

An interesting challenge would be the measurement of diamond films, because diamond possesses an extremely high thermal conductivity of up to 2300 W/(m·K). Diamond films can have grain sizes from some hundred micrometers to a few nanometers. Since smaller grain sizes result in a larger grain boundary area, phonon scattering at grain boundaries is supposed to increase at decreasing grain size. Measuring a series of diamond films and relating measured thermal conductivity values to film properties like the grain size could be an interesting and challenging task.

APPENDIX A

Measuring the film thicknesses of silica films by laser acoustics

Laser acoustics [42, 43] were used to determine the film thickness of the silicon dioxide films. Although originally developed to determine the Young's moduli of thin and hard coatings, it can be extended to measure film thicknesses if film parameters such as density and Young's modulus are known. Laser acoustics offer the advantage of being non-destructive and especially suited to characterize coatings as thin as a few nanometers.

Laser-induced acoustic waves propagate along the surface with a velocity that depends on the elastic properties of the material. In a homogeneous isotropic material the surface acoustic wave (SAW) velocity is constant, while in coated materials the velocity depends on frequency. This frequency dependence is caused by the skin effect resulting in a reduced SAW penetration depth with increasing frequencies. Hence, surface waves with higher frequencies are more influenced by thin films, in a manner similar to the principle of the 3ω method. The dependence of the SAW velocity on the frequency can be plotted as a dispersion curve. The shape of that curve depends on film parameters, i.e. Young's modulus, density, and thickness. The dispersion data is fit to a theoretical curve which allows one to determine the values of the Young's modulus, film thickness and density.

For the SiO_2 films fabricated in this study the dispersion curves follow a straight line for frequencies up to 200 MHz (Figure 24). Therefore, the film thickness of the silica films can be determined directly from the slope of the phase velocity as a function of frequency (Figure 25).

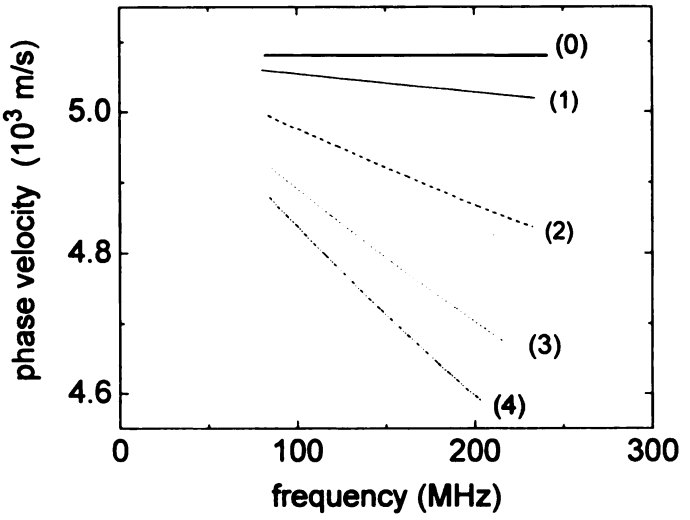

Figure 24. Dispersion curves measured by laser acoustics: Phase velocities for the four SiO_2 films on silicon (Table 5). The plot marked (0) refers to an uncoated silicon substrate.

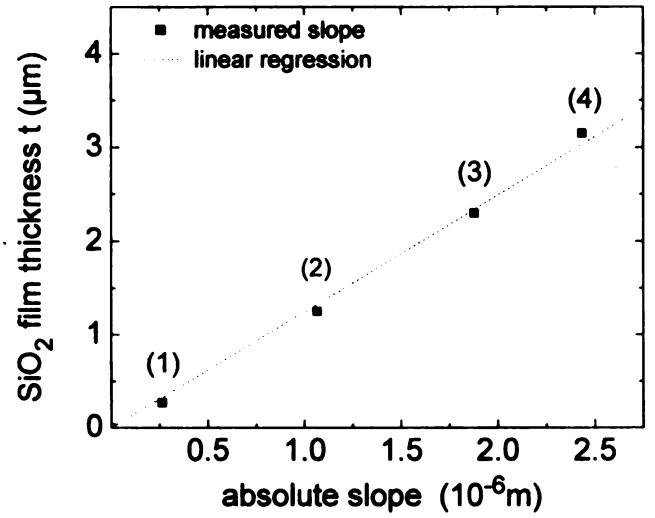

Figure 25. Due to the linear behavior of the phase velocity versus frequency in Figure 24, the slopes of the plots were used to estimate the film thickness *t* of the silica films. A Young's Modulus of 69 GPa and a density of 2200 kg/m³ were assumed for silica in these calculations.

REFERENCES

[1] A. Elshabini, and F.D. Barlow, *Thin film technology handbook*, McGraw-Hill, 1997.

[2] D. Vashaee and A. Shakouri, "Electronic and thermoelectric transport in semiconductor and metallic superlattices", *J. Appl. Phys.* **95**, pg. 1233, 2004.

[3] P.F. Nealey, J.J. de Pablo, M.D. Ediger, and F. Cerrina, "Dimension dependent properties of nanoscopic macromoluecular structures", *Proceedings* NSF Nanoscale Science and Engineering Grantees Conference 2003.

[4] K.E. Goodson, O.W. Käding, M. Rösler, and R. Zachai "Experimental investigation of thermal conduction normal to diamond-silicon boundaries", *J. Appl. Phys.* **77**, pg. 1385, 1995.

[5] K. Jagannadham and H. Wang, "Thermal resistance of interfaces in AlN–diamond thin film composites", *J. Appl. Phys.* **91**, pg. 1224, 2002.

[6] D. Kotchetkov, J. Zou, A.A. Balandin, D.I. Florescu, and F.H. Pollak, "Effect of dislocations on thermal conductivity of GaN layers", *Appl. Phys. Lett.* **79**, pg. 4316, 2001.

[7] D.G. Cahill and R.O. Pohl, "Thermal conductivity of amorphous solids above the plateau", *Phys. Rev. B* **35**, pg. 4067, 1987.

[8] J.E. Graebner, S. Jin, G.W. Kammlott, Y.-H. Wong, J.A. Herb, and C.F. Gardinier, "Thermal conductivity and the microstructure of state-of-the-art chemical-vapor-deposited (CVD) diamond", *Diamond and Related Materials* **2**, pg. 1059, 1993.

[9] J.E. Graebner, "Simple correlation between optical absorption and thermal conductivity of CVD diamond", *Diamond and Related Materials* **4**, pg. 1196, 1995.

[10] D.T. Morelli, T.M. Hartnett, and C.J. Robinson, "Phonon-defect scattering in high thermal conductivity diamond films", *Appl. Phys. Lett.* **59**, pg. 2112, 1991.

[11] F.W. Sears, *An introduction to thermodynamics, the kinetic theory of gases, and statistical mechanics,* 2nd Edition, fifth printing, Addison-Wesley Publishing Company, Inc., 1964.

[12] J.M. Ziman, *Principles of the theory of solids,* Cambridge University Press, 1964.

[13] C. Kittel, *Introduction to Solid State Physics,* John Wiley & Sons, Inc., 6th edition, 1986.

[14] G.A. Slack, "Effect of isotopes on low-temperature thermal conductivity", *Phys. Rev.* **105**, pg. 829, 1957.

[15] G.A. Slack, "Thermal conductivity of CaF_2, MnF_2, CoF_2, and ZnF_2 crystals" *Phys. Rev.* **122**, pg. 1451, 1961.

[16] D.-J. Yao, H.-C. Chien. Y.-C. Liu, and M.-H. Tseng, "The study of thin films thermal conductivity measurement by 3ω method" *Proceedings* International symposium on Nanotechnology and Energy, Hsinchu, Taiwan, ROC, 2004.

[17] H.S. Carslaw and J.C. Jaeger, *Conduction of heat in solids,* Oxford University Press, Oxford, 1959.

[18] W.D. Callister, *Materials Science and Engineering: An Introduction,* John Wiley & Sons, Inc., 2003.

[19] A. Erdelyi (Editor). *Tables of integral Transforms, Vol I,* McGraw-Hill, New York, 1954.

[20] D.G. Cahill, "Thermal conductivity measurement from 30 to 750 K: the 3ω method", *Ref. Sci. Instrum.* **61**(2), pg. 802, 1980.

[21] D.G. Cahill, H.E. Fischer, T. Klitsner, E.T. Swartz, and R.O. Pohl, "Thermal conductivity of thin films: Measurements and understanding", *J. Vac. Sci. Technol.* **A7**, pg. 1259, 1989.

[22] D.G. Cahill, M. Katiyar, and J.R. Abelson, "Thermal conductivity of a-Si:H thin films", *Phys. Rev. B* **50**, pg. 6077, 1994.

[23] D.G. Cahill and S.-M. Lee, "Thermal conductivity of k-Al_2O_3 and a-Al_2O_3 wear-resistant coatings", *J. Appl. Phys.* **83**, pg. 5783, 1998.

[24] S.-M. Lee and D.G. Cahill, "Heat transport in thin dielectric films", *J. Appl. Phys.* **81**, pg. 2590, 1997.

[25] R.M. Costescu, A.J. Bullen, G. Matamis, K.E. O'Hara, and D.G. Cahill, "Thermal conductivity and sound velocities of hydrogen-silsesquioxane low-k dielectrics", *Phys. Rev. B* **65**, pg. 942, 2002.

[26] J.H. Kim, A. Feldmann, and D. Novotny, "Application of the three omega thermal conductivity measurement method to a film on a substrate of finite thickness", *J. Appl. Phys.* **87**, pg. 3959, 1999.

[27] J.R. Olson and R.O. Pohl, "Thermal conductivity of diamond between 170 and 1200 K and the isotopic effect", *Phys. Rev. B* **47**, 1993.

[28] A. Jacquot, B. Lenoir, and A. Dauscher, "Numerical simulation of the 3ω method for measuring the thermal conductivity", *J. Appl. Phys.* **91**, pg. 4733, 2002.

[29] D.R. Lide, *Handbook of Chemistry and Physics,* 84th Edition, CCR Press, LLC, 2004.

[30] E. Wörner, C. Wild, W. Müller-Sebert, R. Locher, and P. Koidl, "Thermal conductivity of CVD diamond films: high-precision, temperature-resolved measurements", *Diamond and Related Materials* **5**, pg. 688, 1996.

[31] D. Fournier and K. Plamann, "Thermal measurements on diamond and related materials", *Diamond and Related Materials* **4**, pg. 809, 1995.

[32] E. Jansen and E. Obermeier, "Thermal conductivity measurements on thin films based on micromechanical devices", *J. Micromech. Microeng.* **6**, pg. 118, 1996.

[33] A.V. Khomich, V.G. Ralchenko, A.V. Vlasov, R.A. Khmelnitskiy, I.I. Vlasov, and V.I. Konov, "Effect of high temperature annealing on optical and thermal properties of CVD diamond", *Diamond and Related Materials* **10**, pg. 546, 2001.

[34] D.J. Twitchen, C.S.J. Pickles, S.E. Coe, R.S. Sussmann, and C.E. Hall, "Thermal conductivity measurements on CVD diamond", *Diamond and Related Materials* **10**, pg. 731, 2001.

[35] S.D. Wolter, D.-A. Borca-Tasciuc , G. Chen, N. Govindaraju, R. Collazo, F. Okuzumi, J.T. Prater, and Z. Sitar, "Thermal conductivity of epitaxially textured diamond films", *Diamond and Related Materials* **12**, pg. 61, 2003.

[36] T.R. Anthony, W.F. Banholzer, J.F. Fleischer, L. Wei, P.K. Kuo, R.L. Thomas, and R.W. Pryor, "Thermal diffusivity of isotopically enriched ^{12}C diamond", *Phys. Rev. B* **42**, pg. 1104, 1990.

[37] E. Wörner, E. Pleuler, C. Wild, and P. Koidl, "Thermal and optical properties of high purity CVD-diamond discs doped with boron and nitrogen", *Diamond and Related Materials* **12**, pg. 744, 2003.

[38] H.P. Ho, K.C. Lo, S.C. Tjong, and S.T. Lee, "Measurement of thermal conductivity in diamond films using a simple scanning thermocouple technique", *Diamond and Related Materials* **9**, pg. 1312, 2000.

[39] J.E. Graebner, M.E. Reiss, L. Seibles, T.M. Hartnett, R.P. Miller, and C.J. Robinson, "Phonon scattering in chemical-vapor-deposited diamond", *Phys. Rev. B* **50**, pg. 3702, 1994.

[40] D.G. Onn, A. Witek, Y.Z. Qiu, T.R. Anthony, and W.F. Banholzer, "Some aspects of the thermal conductivity of isotopically enriched diamond single crystals", *Phys. Rev. Lett.* **68**, pg. 2806, 1992.

[41] K.M. Leung, A.C. Cheung, B.C. Liu, H.K. Woo, C. Sun, X.Q. Shi, and S.T. Lee, "Measuring thermal conductivity of CVD diamond and diamond-like films on silicon substrates by holographic interferometry", *Diamond and Related Materials* **8**, pg. 1607, 1999.

[42] D. Schneider, T. Schwarz, H.-J. Scheibe, and M. Panzner, "Non-destructive evaluation of diamond and diamond-like carbon films by laser induced surface acoustic waves", *Thin Solid Films* **295**, pg. 107, 1997.

[43] M. Leonhardt, D. Schneider, J. Kaspar, and S. Schenk, "Characterizing the porosity in thin titanium films by laser-acoustics", *Surf. Coat. Technol.* **185**, pg. 292, 2004.